Master's Theses and Capstones   Student Scholarship

Winter 2007

Fungal glycosphingolipids: Characterization of structures and interactions with plant defensins

Jis Joe
University of New Hampshire, Durham

Follow this and additional works at: https://scholars.unh.edu/thesis

FUNGAL GLYCOSPHINGOLIPIDS: CHARACTERIZATION OF STRUCTURES

AND INTERACTIONS WITH PLANT DEFENSINS

BY

JIS JOE

BS Chemistry, Mahatma Gandhi University, India, 1995

THESIS

Submitted to the University of New Hampshire

In Partial Fulfillment of

The Requirements for the Degree of

Master of Science

In

Chemistry

December, 2007
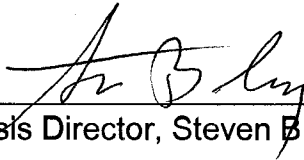
UMI Number: 1449589

UMI®
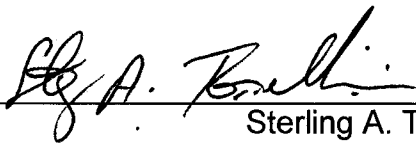
This thesis has been examined and approved.

_____
Thesis Director, Steven B. Levery, Associate Professor

_____
Sterling A. Tomellini, Professor

_____
Arthur Greenberg, Professor

_____13 December 2007_____
Date

TABLE OF CONTENTS

CHAPTER   PAGE

iii

iv

LIST OF TABLES

LIST OF FIGURES

vi

vii

LIST OF SCHEMES

ix

ABSTRACT

FUNGAL GLYCOSPHINGOLIPIDS: CHARACTERIZATION OF STRUCTURES

AND INTERACTIONS WITH PLANT DEFENSINS
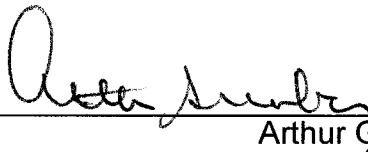
by

Jis Joe

University of New Hampshire, December, 2007

Glycosphingolipids (GSLs) play important roles in many fundamental biological processes like activation of signal transduction pathways, immune responses, and cell-cell interactions. Recent reports imply that fungal GSLs are important targets for the antifungal action of plant defensins. In order to study intermolecular interactions of GSLs, it is crucial to know their structures in detail. This thesis consists of two projects in which fungal GSLs of biological and biomedical significance are studied. In the first project, we have completed the structural characterization of acidic GSLs from *S. cerevisiae* using NMR spectroscopy and electrospray ionization mass spectrometry (ESI-MS). The second project of this thesis is carried out to help understand some of the possible interactions of fungal GSLs with plant defensins. Studies using enzyme – linked immunosorbent assay and mass spectrometry are used to clarify some of the structural requirements for GSL – defensin interactions. These in turn should lead to more general insights into structure – function relationships of GSLs and proteins that bind to them.

x

CHAPTER I

INTRODUCTION

Fungi, plants and animals represent three well-known phylogenetic kingdoms within the eukaryotes (non-bacteria) having similar cellular, genomic and metabolic organizations. Fungi rank in importance with bacteria as agents in the biosphere for biochemical transformations and environmental housekeeping. Along with bacteria and viruses, fungi take part in number of complex interspecies interactions as either symbionts or pathogens. By breaking down dead organic material, they continue the cycling of nutrients through ecosystems. In addition, most vascular plants could not grow without the symbiotic fungi that inhabit their roots and supply essential nutrients. Other fungi provide numerous drugs (such as penicillin and other antibiotics), foods like mushrooms, truffles and morels, and the bubbles in bread, champagne, and beer. Fungi also cause a number of plant and animal diseases. Because fungi are more chemically and genetically similar to animals than other organisms, fungal diseases are very difficult to treat. However, due to these similarities a number of fungi are important model organisms for studying problems in cellular and molecular biology. Because of the many shared characteristics of eukaryotic cell membranes, fungi have been proposed as good model systems for the study of genetics, biosynthesis, organization and functional interactions of membrane components [1, 2, 3]. Among these key components are the sphingolipids,

1

derivatives of sphingolipids, a family of functionalized long-chain alkyls with a defining 1, 3-dihydroxy-2-amino structural motif. The bulk of cellular sphingolipids are incorporated into fatty-N-acylated derivatives called ceramides. Ceramides, in turn, are further used as substrates for a variety of enzymes that catalyze the attachment of polar head groups, such as *myo*-inositol phosphate, choline phosphate, and monosaccharide residues. Attachment of the latter produces glycosphingolipids (GSLs).

Glycosphingolipids

Glycosphingolipids are, together with sterols and glycerophospholipids the major types of lipids found in eukaryotic membranes. GSLs are one of the most abundant components of the fungal plasma membrane, with smaller amounts found in other cellular membranes. Despite their abundance, functional roles of GSLs and other sphingolipids in cellular processes have only begun to be elucidated in recent decades. While significant progress has been made, many specific functions of complex GSLs await elucidation. It has been proven that sphingolipids play important structural and regulatory roles in membranes [2, 3, 4]. Ceramides, basic building blocks of sphingolipids, are reported to be signaling molecules in mammals. Exactly how ceramides activates signal transduction pathways is not well understood, but it is clear that the pathways control many cellular processes including apoptosis, proliferation and differentiation, immune responses, and cell-cell interactions. Established roles of the sphingolipids also include signaling functions during heat stress, mediating transport of glycosyl phosphatidylinositol (GPI)-anchored proteins from endoplasmic reticulum to

2

Golgi, regulating calcium homeostasis, and interactions with sterols that are important for lipid raft formation and function [3, 4]. Interest has been sparked by indications that they play an important role in interactions with plant-derived small antimicrobial peptides, called defensins, which target fungal membrane components [5, 6]. The existence of high affinity binding sites for these defensins on fungal plasma membrane fractions has been demonstrated [7, 8, 9, 10]. Considerable evidence suggests that in most of the cases these binding sites are GSLs, or include GSLs as essential components.

Recent studied have shown that GSLs may be used for sensitive and reliable recognition of certain protein toxins like tetanus toxin and cholera toxin [11]. GSLs have been shown to undergo strong interactions with potential bioterrorism agents such as ricin and botulinum neurotoxin. Attempts have been made to develop biosensors using GSLs as the recognition molecules [21, 31]. Traditionally, antibodies have been used as detection molecules for these types of toxins. However, GSLs offer several potential advantages over antibodies, including increased stability under ambient conditions, ease of orientation at the sensor surface through hydrophobic/hydrophilic interactions, and a large number of binding sites per unit area compared to the larger antibody.

Disruptions in GSL biosynthetic pathways have been shown to inhibit growth and differentiation. Many studies have proven that GSL synthesis is essential for the organization of embryonic tissues. In some inherited pathologies the GSL biosynthetic pathway is intact, but the degradative pathways are not fully functional. This situation leads to a disease state due to inactive enzymes or

3

activators needed for the metabolic degradation of biosynthetic products [13, 14]. Gaining a clearer understanding of GSL structure, biosynthesis, and function will help in treating diseases caused by GSL pathway defects in eukaryotes, as well as diseases mediated by their use as microbial binding sites.

<u>Biosynthetic pathway</u>

Synthesis and expression of sphingolipids seems to be essential for normal processes in fungal and animal cells. Many essential features of the biosynthetic pathways for GSL expression have been established in both animals and fungi. Early steps in both animal and fungal species are similar, but the predominant final products are structurally different. Fungal cells possess some exclusive pathways of sphingolipid biosynthesis, some of which are crucial to cell viability. For that reason, biosynthesis of sphingolipids is emerging as an attractive target for the action of antifungal drugs. Several inhibitors of sphingolipid synthesis in fungi, all natural products and most of them non-toxic to mammalian cells, have been in fact reported in the last decade [12, 15, 16]. This observation agrees with the fact that, between fungal and mammalian cells, glycosphingolipids differ in structure and biosynthesis. The understanding of GSL biosynthesis is, therefore, fundamental for the development of antifungal drugs and for the complete knowledge of lipid function in fungal cells.

All organisms begin sphingolipid synthesis by condensing serine and palmitoyl-CoA to yield 3-ketodihydrosphingosine (see Scheme 1-1). This essentially irreversible reaction is catalyzed by serine palmitoyltransferase (SPT). The genes believed to code for SPT activity is *LCB1, LCB2,* and *TSC3.* Deletion

4

of either *LCB1* or *LCB2* is lethal to the organism. The product of *TSC3* is necessary for optimal SPT activity, since its absence in vitro leads to reduction of SPT activity to a great extent. 3-ketodihydrosphingosine is reduced by an NADPH-requiring reaction yields the long-chain base dihydrosphingosine (sphinganine).The gene *TSC10* has been shown to encode the enzyme, 3-ketodihydrosphingosine reductase, necessary for the formation of sphinganine in sphingolipid synthesis. Next, a fatty acid, generally between 16 and 26 carbons long, is then amide-linked to dihydrosphingosine to yield dihydroceramide. This reaction is catalyzed by dihydrosphingosine *N*-acyltransferase (ceramide synthase) enzyme, whose activity is coded by two genes, *LAG1* and *LAC1*. A deletion of either gene is not lethal to the organism, but the cells grow poorly. Hydroxylation of C_4 of the dihydrosphingosine moiety of dihydroceramide yields a ceramide containing the long-chain base phytosphingosine. On the other hand, dehydrogenation at C_4-C_5 produces a ceramide containing the long-chain base referred to as sphingosine. The *SUR2*/*SYR2* gene is necessary for hydroxylation of dihydrosphingosine. In general, ceramides comprise a large, diverse family of N-acylated derivatives of sphingoids, where sphingoid is any long-chain hydrocarbon with a 2-amino-1,3-dihydroxy functional motif [2, 3, 4, 9]. Scheme 1-1 shows some of the important steps in biosynthetic pathway for the formation of ceramides. Glycosylation of ceramide, or a ceramide derivative called *myo*-inositol phosphorylceramide (IPC), yields GSLs.

5
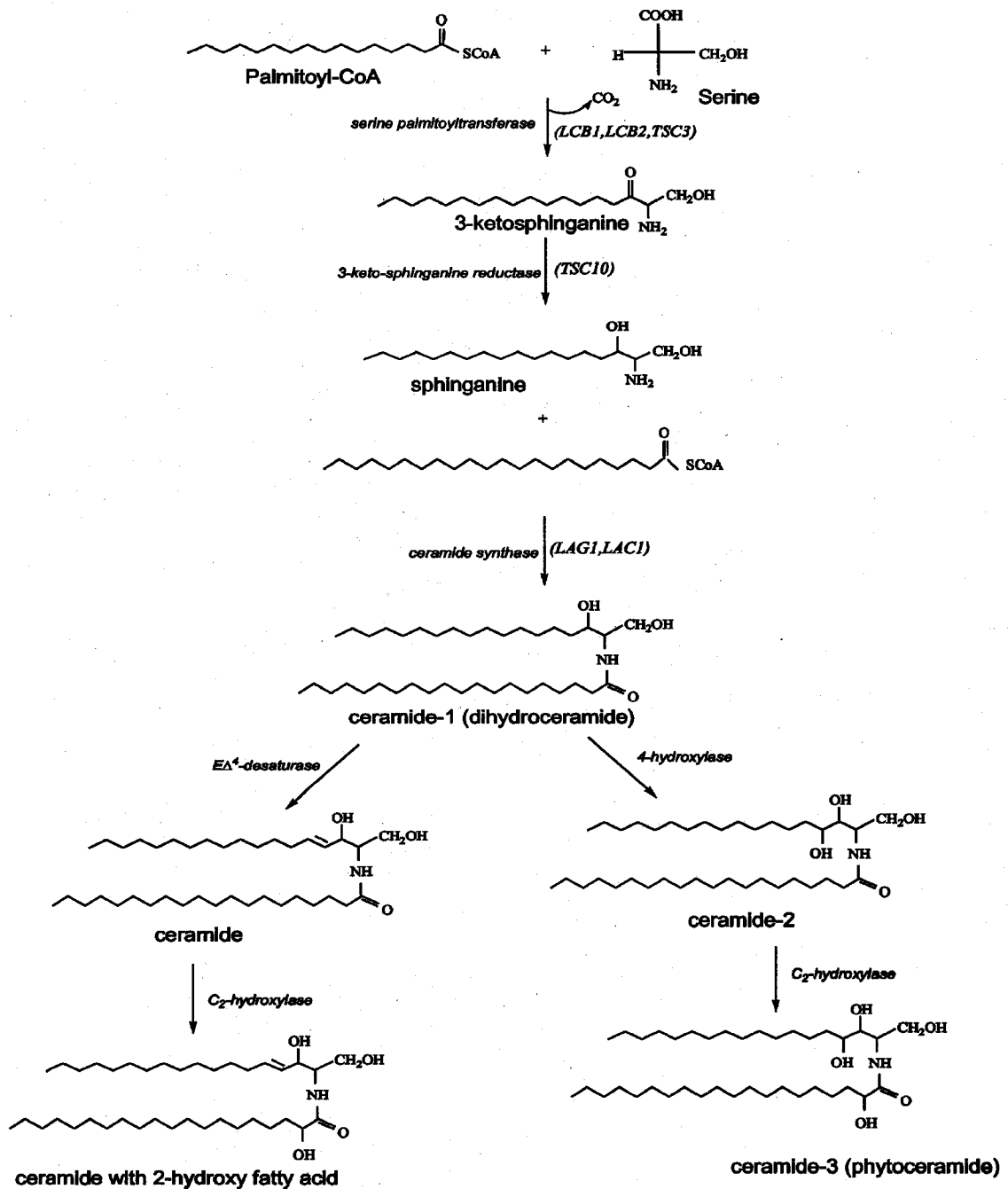
Scheme 1-1: GSL biosynthetic pathway

Two general groups of GSLs are known in fungi and they are

distinguished from each other by the relation of their carbohydrate to the

6

ceramide moiety. While only a small number of fungi have been examined, most

contain GSLs composed of ceramide derivatized at O-1 with *myo*-inositol-1-

phosphate (IPC). The *myo*-inositol is then glycosylated by the sequential action

of glycosyltransferases, generally beginning at O-2 or O-6 of the inositol moiety.

Typical glycosyl residues include mannose (Man), galactose (Gal), fucose (Fuc),

and xylose (Xyl). These compounds are commonly called glycosylinositol

phosphorylceramides (GIPCs) [18, 19]. In general, GIPCs are not found in

mammalian cells or tissues, but are characteristic GSL components of fungi and

plants. Many studies have shown that GIPCs are essential for the survival of

fungi [17]. A representative structure of a simple GIPC is given in Figure 1-1. A

total of ~ 30 distinct GIPC structures have been identified to date, with the

discovery rate increasing during the last 5-6 years.
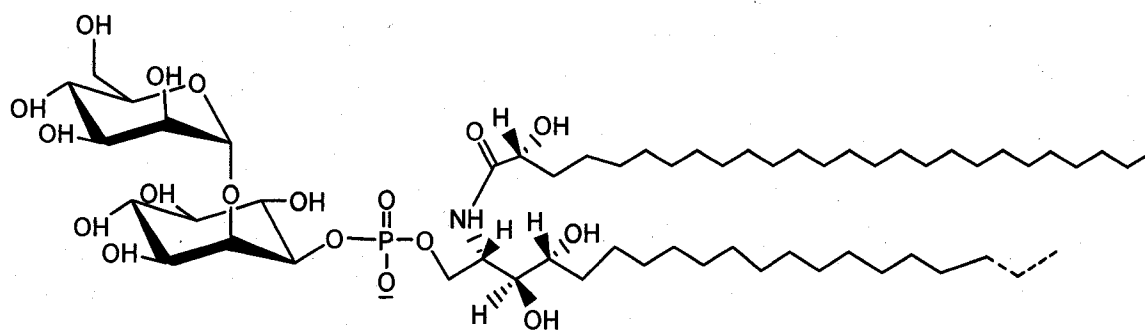
Figure1-1: Representative structure of GIPCs (α-mannosyl inositol
phosphorylceramide)

Biosynthesis of fungal GIPCs starts with the transfer of *myo*-inositol-1-

phosphate (IP) from the diacylglycerol (DAG) moiety of phosphatidylinositol to

ceramide. This reaction is catalyzed by the *AUR1* gene family-encoded enzyme

7

IPC synthase. In many fungi, the common intermediate Mα2IPC is next synthesized by the action of an α 1,2-mannosyl transferase (Mα2-T). In *Saccharomyces cerevisiae,* this enzyme is encoded by either *SUR1/CSG1* or *CSG2*, or both genes; next, the *IPT1* encoded protein transfers a second *myo-*inositol-1-phosphate from phosphatidylinositol to Mα2IPC forming IP6Mα2IPC. In many other fungi, an as yet unknown Mα3-T transfers a second α-Man residue to Mα2IPC to make a common intermediate Mα3Mα2IPC [17]. Scheme 1-2 shows the structure and biosynthesis of some fungal GIPCs.
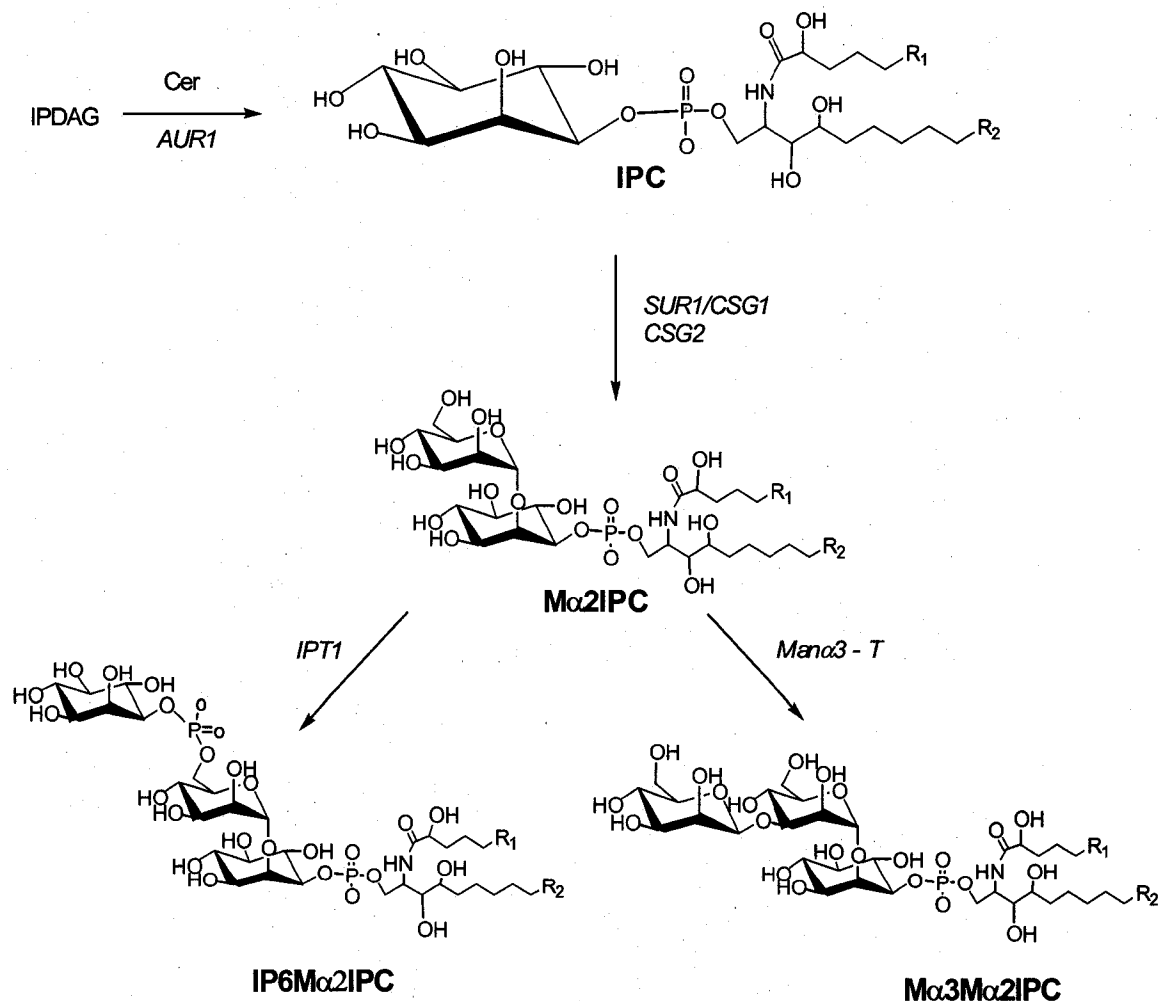
Scheme 1-2: Biosynthesis of fungal GIPCs starting with transfer of IP to ceramide.

8

The second major class of fungal GSLs is the monohexosylceramides, having either β-glucose or β-galactose attached directly to the ceramide to generate β-glucosyl ceramide or β-galactosyl ceramide (GlcCer or GalCer, respectively). Fungal glycosylceramides are much conserved structures, in which modifications include different sites of unsaturation as well as the varying length of fatty acid residues in the ceramide moiety. They usually contain a ceramide moiety with 9-methyl-4,8-sphingadienine amide linked to 2-hydroxyoctadecanoic or 2-hydroxyhexadecanoic acids. Fungal glycosylceramides sometimes contain additional sugar residues, but are more commonly encountered as terminal products. These molecules are formed through the action of UDP-glycosyl ceramide glycosyltransferases (glycosylceramide synthases). Some fungi have been shown to produce both GlcCer and GalCer while others only produce GlcCer [13, 14]. The structure of a fungal monohexosyl ceramide is represented in Figure 1-2.
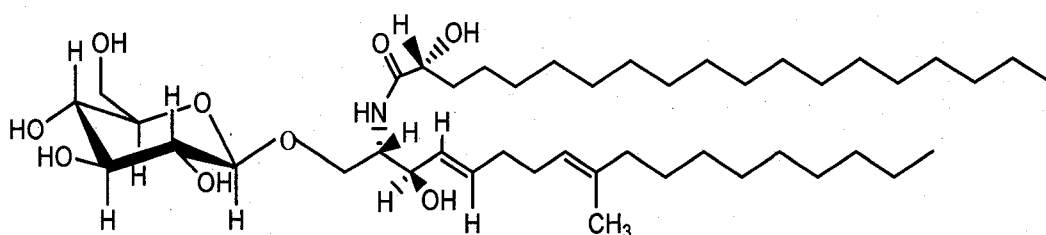
Figure 1-2: Representative Structure of GSLs (β-D-glucosylceramide)

Based on numerous studies, fungal cells are believed to have two different pools of ceramides to be used for the synthesis of different sphingolipids.

9

Ceramide backbones with C16 or C18 α-hydroxy fatty acids linked to a 4, 8-diene-9-methyl-sphingoid, widely identified in several fungal species, are thought to be exclusively used as precursors of glycosylceramide synthesis. In contrast, ceramide backbones with relatively long chain C24 and C26 α-hydroxy fatty acids bound to phytosphingosine are thought to be restricted to the synthesis of the *myo*-inositol containing phosphosphingolipids [35].

On the other hand, in other eukaryotes, such as animal species, GlcCer and GalCer are generally not accumulated, but further glycosylated to form a wide variety of complex GSLs. The great diversity of mammalian GSL glycans results in large part from mixing and matching the core structures with the peripheral and side-chain monosaccharide residues. Additional diversity in molecular species structure often derives from the occurrence of a distribution of multiple ceramide forms attached to each glycan in the GSL pool. In mammals GlcCer and GalCer are inherently important for a number of reasons. It has been suggested that glycosylation of ceramide can protect mammalian cells from cancer drug-induced apoptosis [1]. Accumulation of GlcCer was observed in another study of multidrug-resistant tumor cells [10]. These findings support the idea that ceramide may be a second messenger in stress responses and apoptosis.

Importance of Characterizing GSLs of Fungi

Studies carried out during the 1990s demonstrated that many species of fungi are vulnerable to inhibitors of sphingoid biosynthesis. This has stimulated increased interest in the structure, biosynthesis, and functional roles of fungal

sphingilipids. Fungal GSLs, as well as the cellular machinery regulating their expression are potential targets for the diagnosis and treatment of fungal diseases. This is important because of the dramatic increase in the frequency of severe mycotic infections and resistance to available antifungal agents during the past two decades. This situation has created an urgent need for new antifungal therapeutic and diagnostic agents, and by extension, an imperative to identify components that are not only critical to fungal life cycle and infectivity but that also contain structural elements distinct from those of the host. Since GIPCs generally are not synthesized by mammals, they represent promising targets for antifungal drug development. While the exact functions of GIPCs are still being studied, it appears GIPCs are an essential requirement for the survival of fungi. A particularly interesting target is the fungal IPC synthase, inhibitors of which are highly toxic to many mycopathogens but exhibit low toxicity in mammals [14, 15]. IPC synthase catalyzes the transfer of *myo*-inositol-1-phosphate from phosphatidylinositol to ceramide. If further steps in the biosynthetic pathway of GIPCs are identified as essential, the enzymes catalyzing these reactions, glycosyltransferases, may also be potential targets of inhibitory drugs.

In the past, a number of studies have targeted fungal cell wall proteins, glycoproteins, and polysaccharide components as this has been thought to be the location for direct host-pathogen interaction [25, 27]. GSLs are known to have the potential to induce strong immunological responses in the host when they incorporate structural features different from those of the host [24]. Isolation and detailed characterization of GSLs from a variety of fungi has begun to reveal an

11

extensive structural diversity, the expression of which is considerably dependent on species and at least in some mycopathogens, strongly regulated during morphogenesis. Antigenic glycoside determinants are expressed on some fungal GSL components, suggesting their potential as targets for immunodiagnostic reagents and the possibility of therapy based on stimulation of the mammalian humoral response. Elucidation of such immunological interactions calls for further detailed knowledge of the structures of these compounds, which is still limited compared with what is known about GSLs of animal species.

This thesis consists of two projects in which fungal glycosphingolipids (GSLs) of biological and biomedical significance are studied. The first project in this thesis, described in chapter 2, was aimed at completing the structural characterization of GSLs from the yeast species *Saccharomyces cerevisiae*. In this work, we completed characterization of two GIPCs from *S. cerevisiae* using one- and two-dimensional (1-D and 2-D) NMR spectroscopy and electrospray ionization mass spectrometry (ESI-MS).

The second project of this thesis, described in chapter 3, was carried out to help understand some of the possible interactions of fungal GSLs with plant defensins. Defensins are small peptides with conserved structural motifs expressed in species from all eukaryotic kingdoms. Many of these have antimicrobial activity, and several have strong antifungal activity [22, 24]. Structural determinants in plant defensins that govern their antifungal activity and the mechanisms by which they inhibit fungal growth remain unclear. Studies using enzyme – linked immunosorbent assay (ELISA) and mass spectrometry

12

were proposed to clarify some of the structural requirements for GSL – defensin

interactions. These in turn should lead to more general insights into structure –

function relationships of GSLs and proteins that bind to them.

13

CHAPTER II

STRUCTURE ELUCIDATION OF GLYCOSPHINGOLIPIDS FROM
Saccharomyces cerevisiae

Introduction

The hemiascomycete fungus *Saccharomyces cerevisiae* (baker's yeast) will likely be the first organism in which all genes necessary for sphingolipid metabolism are identified, although its repertoire is limited. Even though we have a fair understanding of the possible roles of sphingolipids in *S. cerevisiae*, the mechanisms at the molecular level leading to these functions are not clearly understood. *S. cerevisiae* only makes complex sphingolipids that contain *myo*-inositol. These are inositol-phosphorylceramide (IPC), mannose-inositol-phosphorylceramide (MIPC) and mannose-di-(inositol-phosphoryl)-ceramide (M(IP)$_2$C) [3, 4]. Although the polar headgroups of animal and fungal GSLs are fundamentally different, the pathways for ceramide biosynthesis have many common features, with key homologous genes shared between them. For this reason, *S. cerevisiae,* a widely used laboratory model, is considered relevant for unraveling the roles and molecular mechanism in signaling, membrane structure and functional interactions in all eukaryotes.

The three complex sphingolipids in *Saccharomyces cerevisiae* are located primarily in the plasma membrane where they account for 30% of plasma membrane phospholipids, which is about 7-8% of the total mass of the

14

membrane. $M(IP)_2C$, the terminal sphingolipid, accounts for about 75% of the mass of total sphingolipids; the remainder are IPC and MIPC [2, 3, 4]. Because of their large mass and large negative charge they are likely to have general effects on processes that are dependent upon the plasma membrane. Whether these sphingolipids are concentrated in the inner leaflet or in the outer leaflet of the plasma membrane is not known.

IPC in *S. cerevisiae* is formed by addition of *myo*-inositol phosphate to ceramides, a reaction catalyzed by IPC synthase whose activity requires the *AUR1* gene. Deletion or inhibition of IPC synthase is fatal for *S. cerevisiae*. IPC is mannosylated to yield MIPC, a reaction that requires the *SUR1* and *CSG2* genes. The terminal step requires the *IPT1* gene, which catalyzes the addition of inositol phosphate to MIPC to yield $M(IP)_2C$ [4]. Studies have shown that *IPT1*mutant cells lack $M(IP)_2C$ in their membrane and are drug-resistant. Such mutant cells are also resistant to an antifungal plant defensin produced by species of dahlia [9]. Recently it was proven that this defensin-sensitivity is not linked with the presence of a nonfunctional *IPT1*-encoding protein but with the presence of $M(IP)_2C$ in the fungal plasma membrane [12]. Monohexosyl ceramides like GlcCer or GalCer have never been found in *S. cerevisiae* under various culture conditions. This is in contrast with many fungal and yeast species in which both inositolphosporyl-containing sphingolipids and significant amounts of glycosylceramides have been detected.

Recent reports imply that $M(IP)_2C$ is implicated in interactions with components of plant immune systems [26, 29]. The specific role of $M(IP)_2C$ in the

15

antifungal action is an intriguing problem waiting to be solved. In order to study intermolecular interactions of *S. cerevisiae* GIPCs, it is crucial to know their structures in detail. While the ceramide structures are well known, detailed data precisely specifying the primary linkage sequence of the polar groups of MIPC and M(IP)$_2$C have never been published. Preliminary studies suggest that the complex sphingolipids of *S. cerevisiae,* IPC, MIPC, and M(IP)$_2$C, are not monomolecular species, but each is a mixture differing in the chain length of both the long chain base and/or the fatty acid. To fully understand how sphingolipid metabolism is integrated with other cellular metabolism, and how these compounds contribute to the various cellular functions, these structural details need to be established.

Experimental Methods

^{1}H- and ^{13}C- Nuclear magnetic resonance spectroscopy (NMR)

Previously isolated and purified underivatized GIPC samples were obtained from Professor Robert L. Lester, University of Kentucky. They were deuterium exchanged by repeated lyophilization from D$_2$O, and then dissolved in 0.5mL DMSO-*d6*/2% D$_2$O for NMR analysis. 1-D ^{1}H NMR , 2-D ^{1}H-^{1}H gradient enhanced correlation (gCOSY),^{1}H-^{1}H total correlation (TOCSY), and ^{1}H -^{13}C- gradient enhanced heteronuclear single quantum coherence (gHSQC) experiments were performed at 35 °C on a Varian Unity Inova 500 MHz spectrometer using standard acquisition software available in the Varian VNMR software package.

16

Positive ion mode ESI-MS analysis

Mass spectrometric analysis was performed on lipid samples using electrospray ionization mass spectrometry (ESI-MS) following lithium ion cationization [19]. For generation of $[M(Li)_2+Li]^+$ and $[M(Li)+Li]^+$ adducts of GIPC molecular species, lithium iodide (10mM) was added to the lipid samples dissolved in methanol until the observed ratio of $[M(Li)+Li]^+$ adducts to mixed Na^+/Li^+ adducts in MS profile mode was >5:1(~ 4:1 in case of $M(IP)_2C$). The necessary LiI concentration was generally in the range of 3 to 5 mM. Mass spectrometry was performed on a Finnigan LTQ equipped with Advion Triversa Nanomate ESI chip in the positive ion mode with a spray voltage of 1.4 kV.

Results and Discussion

NMR spectroscopic analysis of MIPC and M(IP)₂C samples

In Figure 2-1 is reproduced the relevant downfield section of the1-D ^{1}H-NMR spectrum of MIPC from *S.cerevisiae.* Previously published NMR data for an authentic Manα2IPC isolated under identical conditions from the mushroom *A. blazei* was used for comparison [15]. Signals with the same chemical shifts and splitting patterns are visible in the spectrum of MIPC from *S.cerevisiae.* The anomeric proton signal of MIPC was observed at 5.040 ppm versus 5.041 ppm previously observed in Manα2IPC. *myo*-inositol H-5 and H-3 signals were observed at 2.947ppm and 3.221ppm, which in Manα2IPC were previously assigned at 2.956ppm and 3.222ppm respectively. Chemical shift/connectivity

17

assignments of all ^{1}H and ^{13}C signals in the monosaccharide, inositol and the proximal part of the ceramide are performed by sequential application of 2-D ^{1}H-^{1}H COSY, ^{1}H-^{1}H TOCSY, and ^{1}H-^{13}C gHSQC NMR experiments (spectra shown in Appendix A). The complete chemical shift assignments for MIPC from *S.cerevisiae* and *A. blazei* are listed for comparison in Table 2-1. All three residues in the *S.cerevisiae* compound were recognizable by their connectivity/coupling patterns. In particular, *myo*-inositol presents as a cyclic ^{1}H spin system with all hydroxyl groups equatorial except that at C-2; therefore, all 3-bond coupling constants between the non-exchangeable ring protons are in the range of ~9 – 12 Hz, except H -1/H -2 and H -2/H -3, which are ~ 1.5 – 2.5 Hz. The downfield shift increments observed for Ins H-1, H-2 and H-3 of *S.cerevisiae* MIPC, compared with the same resonances in IPC of *A. fumigatus* ($\Delta\delta$ (H-1) = 0.130ppm; $\Delta\delta$ (H-2) = 0.168 ppm; $\Delta\delta$ (H-3) = 0.019 ppm), correlates with α-mannosylation at Ins O-2 [17]. All other ^{1}H and ^{13}C chemical shifts are consistent with the Manα2IPC structure [15]. Thus, data obtained from NMR spectroscopy suggest that the structure of MIPC in *S.cerevisiae* is authentic Manα1 →2Ins1← P→1Cer. See Figure 2-2.
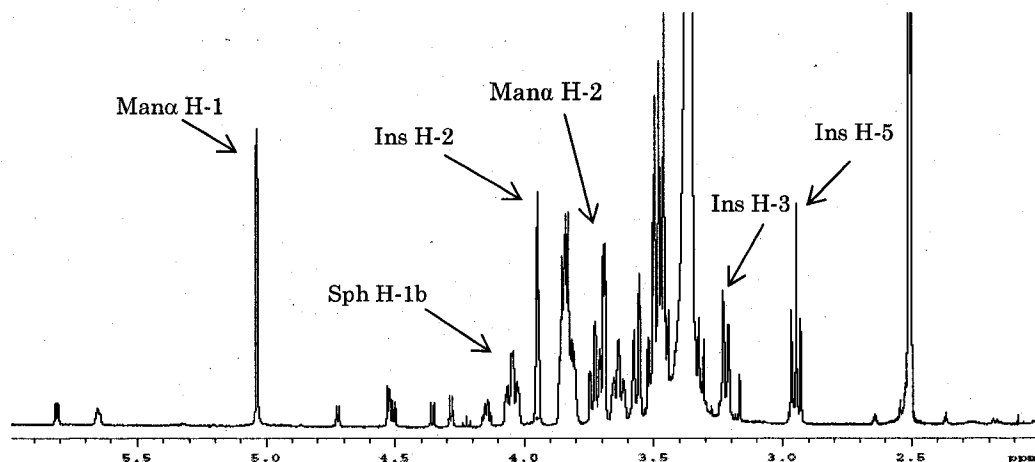
Figure 2-1: Downfield section of 1-D ^{1}H-NMR spectrum of Mα2IPC. Low amplitude signals (<1H) between 4.1 and 4.8 ppm, and above 5.6ppm are incompletely exchanged hydroxyl protons.

Table 2-1

Comparison of ^{1}H and ^{13}C chemical shifts (ppm) for monosaccharide, inositol, ceramide sphingoid and fatty acyl (in parentheses) residues of Mα2IPC from *S. cerevisiae* and *A. blazei* in DMSO-d_6/2% D_2O at 308 K (35 °C)

	S. cerevisiae				*A. blazei*			
	Manα1→2Ins1←P→1Cer				Manα1→2Ins1←P→1Cer			
H-1	5.040	3.729	3.692	4.046	5.041	3.742	3.656	4.048
H-2	3.693	3.952	3.843		3.696	3.965	3.839	
H-3	3.502	3.221	3.463		3.510	3.222	3.470	
H-4	3.473	3.326	3.367		3.468	3.341	3.360	
H-5	3.851	2.947			3.851	2.956		
H-6	3.448	3.483			3.487	3.487		
H-6'	3.567				3.572			
C-1	100.56	75.69	64.02		100.60	75.71	64.05	
C-2	70.34	77.81	50.30	(71.07)	70.35	77.84	50.35	(71.13)
C-3	70.65	70.41	72.52		70.71	70.44	72.82	
C-4	66.60	72.07	70.29		66.70	72.11	70.35	
C-5	72.74	75.53			72.82	74.49		
C-6	60.90	71.31			60.93	72.41		

19
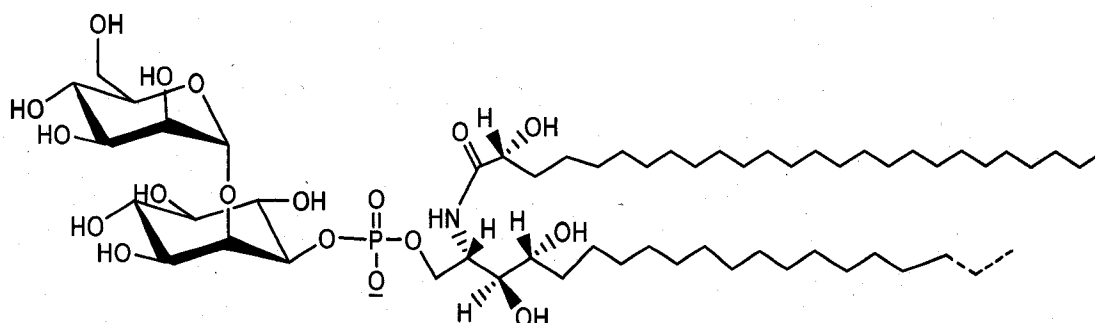
Figure 2-2: Representative structure of MIPC (α-mannosyl inositol phosphorylceramide)

With the data from MIPC in hand, and using analogous NMR methodology, the structure of M(IP)$_2$C was elucidated. The relevant downfield section of the 1-D ^{1}H-NMR spectrum of M(IP)$_2$C is shown in Figure 2-3. Complete assignments of relevant ^{1}H and ^{13}C resonances and connectivities were performed via 2-D spectroscopy. A relevant downfield section of the 2-D ^{1}H-^{1}H TOCSY spectrum of M(IP)$_2$C is given in Figure 2-4. Particularly, in the 2-D ^{1}H-^{1}H TOCSY spectrum of M(IP)$_2$C, two parallel cyclic spin systems corresponding to two inositol residues were clearly observed. The substantial downfield chemical shift increments of H-6 and H-6' of the Man residue in M(IP)$_2$C (Δδ= +0.360 and +0.420 ppm respectively) indicates an electronegative substituent at the C-6 position. This is consistent with a terminal inositol linked to C-6 of Man via the PO$_3$ group. From the observed shift of C-6 (Δδ= +3.78 ppm) and of C-5 (Δδ= -0.81 ppm) of the Man residue in M(IP)$_2$C compared with spectral data for MIPC, it is evident that terminal inositol is linked to C-6 of Man via the PO$_3$ group. This is consistent with the inductive effect of substitution on a monosaccharide, which can affect the chemical shift of the linkage carbon by ~ 4 ppm downfield (α- effect), and the adjacent carbon by ~1 ppm upfield (β-effect).

20

Based on these considerations the structure of M(IP)$_2$C is established as Ins1←

P→ 6Mα1→2Ins1← P→1Cer from its NMR spectra. The chemical shift

assignments for M(IP)$_2$C are given in Table 2-2, along with the proposed

structure (Figure 2-5).

The bulk CH$_2$ resonance (1.234 ppm), representing the carbons between

the terminal methyl groups and the functionalized groups, is difficult to integrate

precisely. In any case, this represents a composite total for which there is no

basis for assigning a specific distribution between the fatty acyl and sphingoid

alkyl chains. Therefore these features for MIPC and M(IP)$_2$C were further

analyzed and defined by ESI-LIT-MS, as described in the next section.
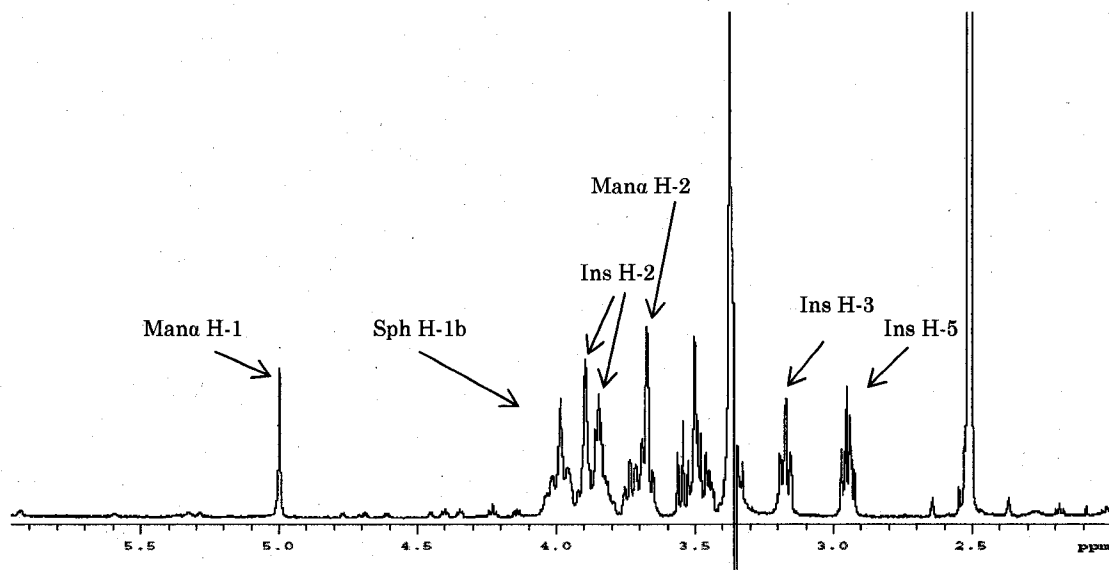
Figure 2-3: Downfield section of 1-D ^{1}H-NMR spectrum of IP6Mα2IPC

21
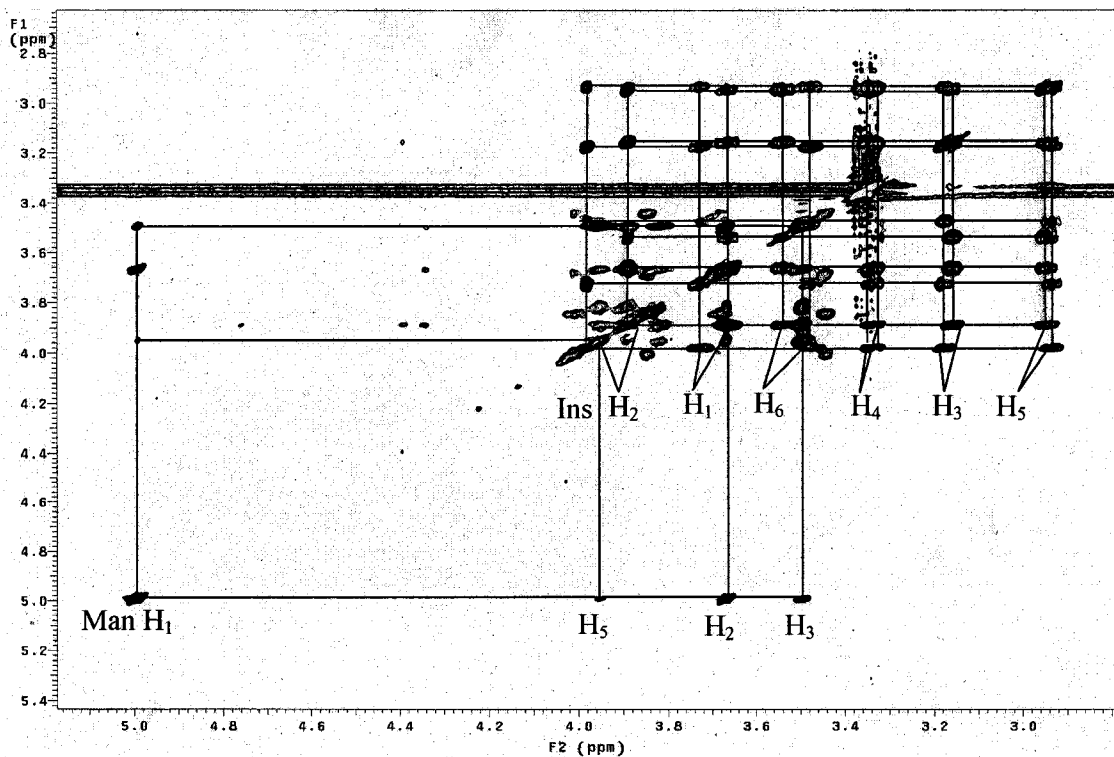
Figure 2-4: Downfield section of 2-D ^{1}H-^{1}H TOCSY- NMR spectrum (200 msec mixing time) of IP6Mα2IPC in DMSO-*d6*/2% D2O at 308 K (35 °C) showing strong inter residue correlations for two cyclic spin systems corresponding to two inositol residues along with mannose and the proximal part of ceramide spin systems.

22

Table 2-2

^{1}H and ^{13}C chemical shifts (ppm) for inositols, monosaccharide, ceramide sphingoid and fatty acyl (in parentheses) residues of IP6Mα2IPC from *S. cerevisiae*, in DMSO-d_6/2% D$_2$O at 308 K (35 °C)

	Ins1←P→6Manα1→2Ins1←P→1Cer				
H-1	3.890	4.993	3.729	3.667	4.007
H-2	3.667	3.671	3.984	3.843	
H-3	3.170	3.499	3.176	3.467	
H-4	3.338	3.346	3.340	3.366	
H-5	2.947	3.952	2.935		
H-6	3.499	3.808	3.475		
H-6'		3.987			
C-1	75.71	100.57	75.90	64.09	
C-2	71.78	70.38	77.78	50.31	71.10
C-3	71.37	70.41	70.60	72.42	
C-4	72.10	66.68	71.78	70.31	
C-5	75.43	71.93			
C-6	72.94	64.68			
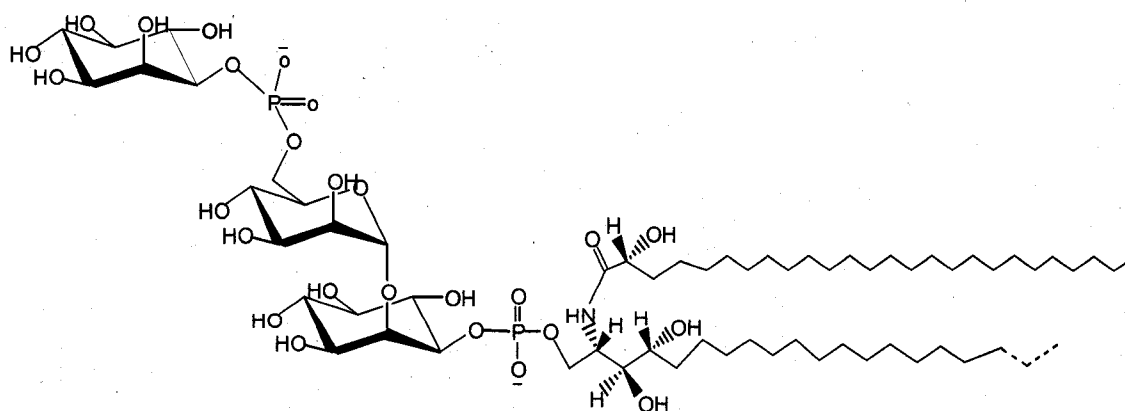
Figure 2-5: Proposed structure of IP6Mα2IPC

23

ESI-MS analysis of MIPC and M(IP)$_2$C samples

Further characterizations, particularly of the ceramide moiety of the MIPC and M(IP)$_2$C samples, were carried out using electrospray ionization-linear ion trap mass spectrometry (ESI-LIT-MS). Nominal monoisotopic m/z values are used in the labeling and description of ESI-MS analysis. The major molecular ion species in the ESI-MS[1] profile of the lithiated adducts for MIPC, [M(Li)+Li]$^+$, were observed at m/z 1128 and 1156 (Figure 2-6). Selected MS^n spectra from [M(Li)+Li]$^+$ adducts are shown in Figures 2-7A and 2-7B (for m/z 1128), and in Figures 2-8A and 2-8B (for m/z 1156).

The two molecular adducts differ by m/z 28, corresponding to ceramide variants differing by 2xCH$_2$ from each other in either the fatty acyl or sphingoid components or both. m/z 1128 is consistent with a GIPC containing of one hexose, one inositol, and one phosphate residue bound to a t18:0/h26:0 or t20:0/h24:0 ceramide moiety. The former has been reported for GIPCs of *S. cerevisiae* (Ceramide III) [51, 52, 53]. MS^2 analysis of the m/z 1128 molecular ion yielded ceramide related product ions at m/z 718 ([Cer + Li]$^+$) and m/z 786 ([CerPO$_3$(Li) + Li]$^+$) (Figure 2-7A). A less abundant fragment observed at m/z 966 represents the residue [Ins•PO$_3$(Li)•Cer + Li]$^+$ indicating loss of mannose from the m/z 1128 molecular ion. A pair of fragments observed at m/z 417 and 435 are consistent with the residue formula ([Hex•Ins•P•Li$_2$]$^+$). In MS^3, m/z 718 further fragments to m/z 291 and m/z 324, which are consistent with a t18:0/h26:0 ceramide moiety (Figure 2-7B).These fragments have been observed consistently in the product ion spectra of ceramides from GIPCs containing t18:0

24

sphingosine [19, 20]. The structure of the m/z 291 ion corresponding to t18:0

sphingosine is shown in Figure 2-9. A fragmentation scheme for m/z 1128 of

MIPC is shown in Scheme 2-1.

MS^2 analysis of the molecular ion at m/z 1156 yielded ceramide related

product ions at m/z 746 ($[Cer + Li]^+$) and 814 ($[CerPO_3(Li) + Li]^+$), which have

an increment of m/z 28 from m/z 718 and 786 respectively (Figure 2-8A). The

residue $[Ins \cdot PO_3(Li) \cdot Cer + Li]^+$) was observed at m/z 994 with an increment of

m/z 28 from m/z 966. The ceramide related precursor ion at m/z 746 further

fragments to m/z 319 and m/z 352 (Figure 2-8B), consistent with a t20:0/h26:0

ceramide moiety. From the observed sequential fragmentation pattern it was

concluded that the ceramide moieties in MIPC consist primarly of a fatty acyl

chain of h26:0 with a mixture of t18:0 and t20:0 phytosphingosines.
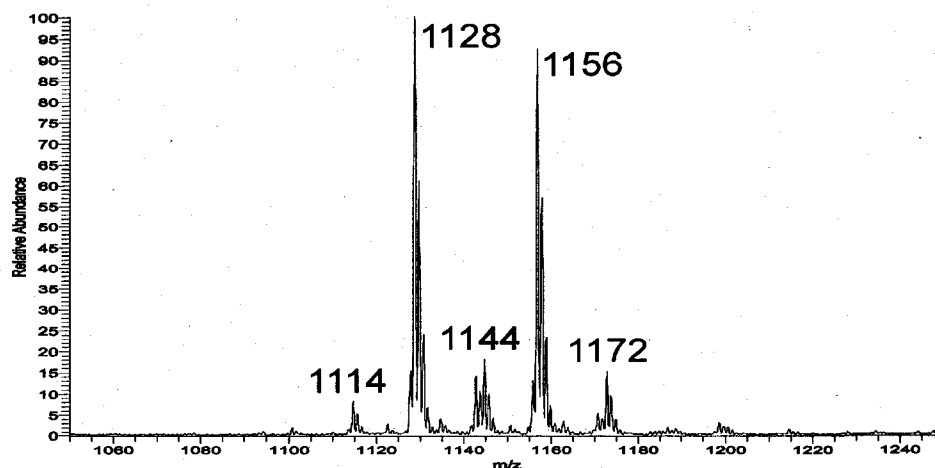
Figure 2-6: ESI-MS^1 Molecular profile of $[M(Li)+Li]^+$ adducts of MIPC.

25

A
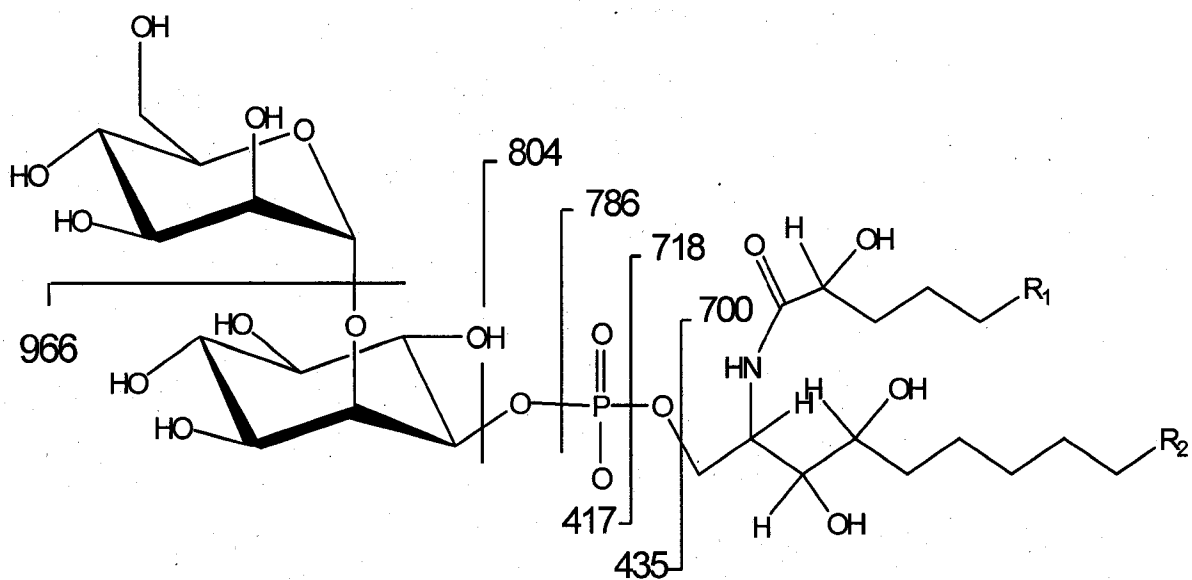
B
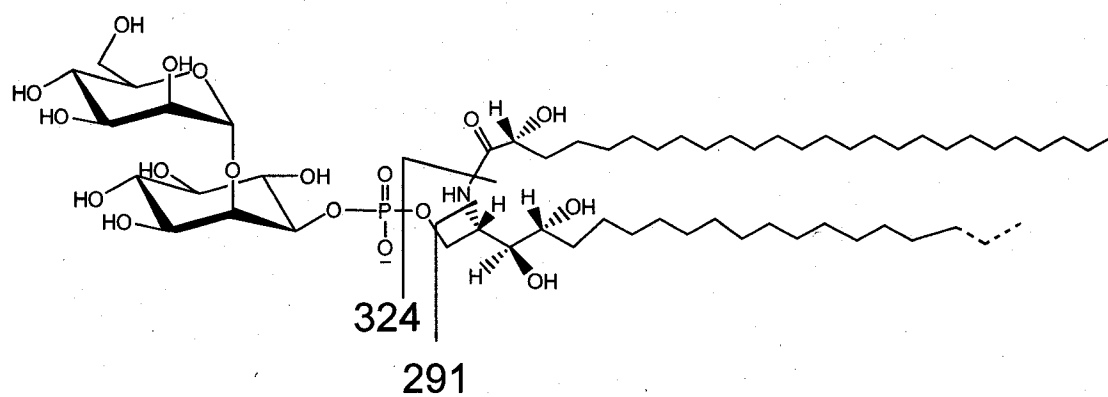
Scheme 2-1: Characteristic fragmentations of the *m/z* 1128 of [M(Li)+Li]$^{+}$ adduct of MIPC.

26
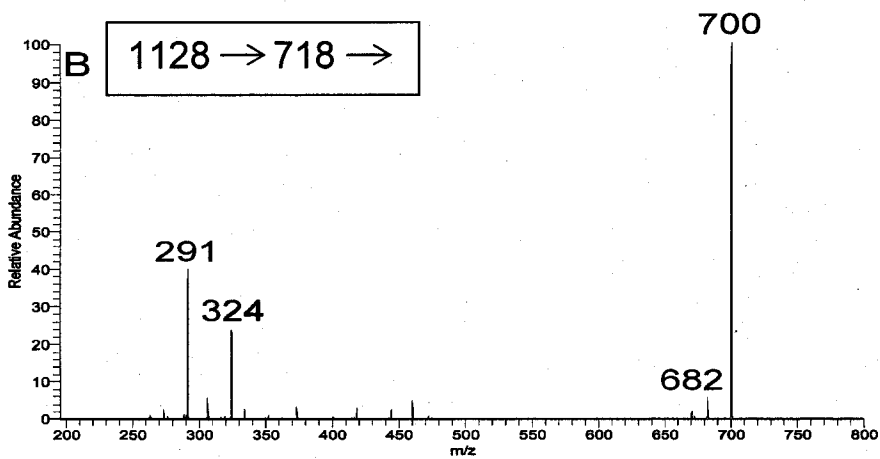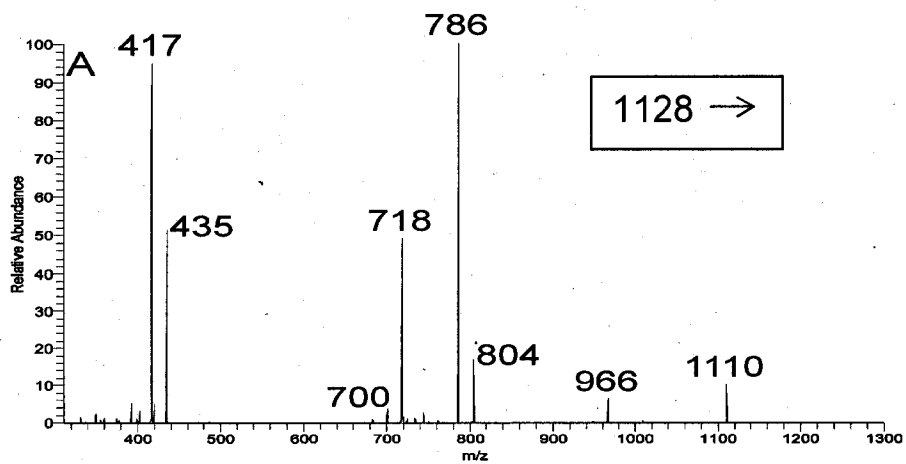
Figure 2-7: MS^2 and MS^3 analysis of the [M(Li) +Li]$^+$ adduct of MIPC *m/z* 1128 (Panels A and B, respectively).

27
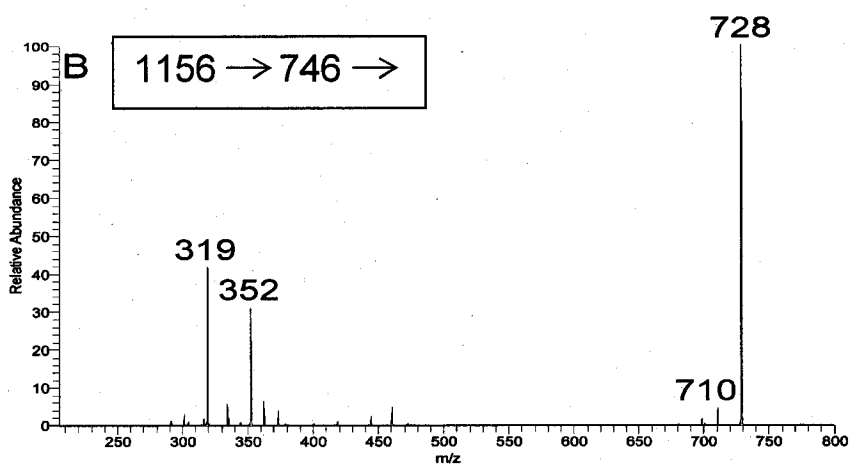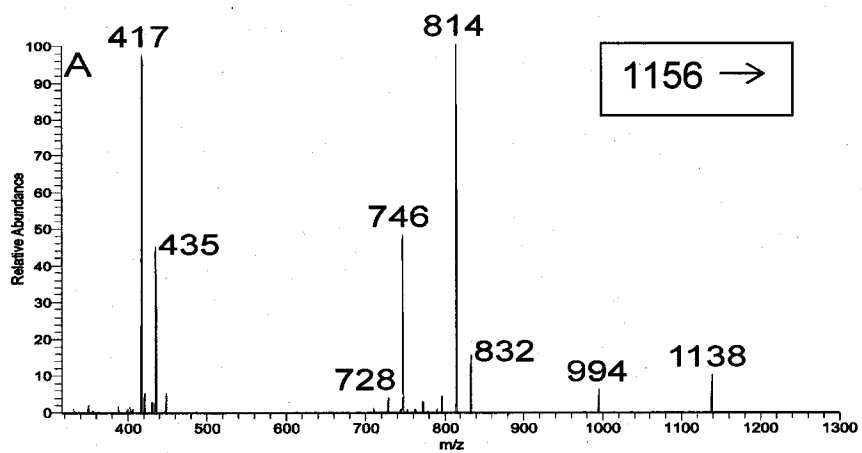
Figure 2-8: MS^2 and MS^3 analysis of the [M(Li) +Li]$^+$ adduct of MIPC *m/z* 1156 (Panels A and B, respectively).

28
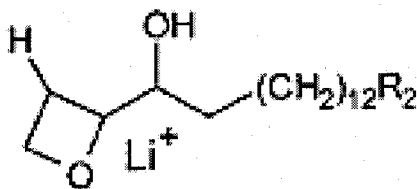
Figure 2-9: Structure of the sphingoid ion corresponding to m/z 291 from the t18:0 sphingosine - containing ceramide.

The major molecular ion species in the ESI-MS profile of the lithiated salt adducts for $M(IP)_2C$, $[M(Li)_2+Li]^+$, were observed at m/z 1376 and 1404 (Figure 2-10). Fragmentation schemes of $M(IP)_2C$ are shown in Schemes 2-2A and 2-2 B. MS^n spectra from selected $[M(Li)_2+Li]^+$ adducts are shown in Figures 2-11 A, B and C (m/z 1376), and 2-12 A, B and C (m/z 1404).

The molecular ion observed at m/z 1376 is consistent with a GIPC consisting of one hexose, two inositol, and two phosphate residues bound to a t18:0/h26:0 or t20:0/h24:0 ceramide moiety. MS^2 analysis of m/z 1376 yielded an abundant fragment at m/z 1128 for ($[Hex \cdot Ins \cdot P \cdot Li_2]^+ + [Cer + Li]^+$) (Figure 2-11A) , which represents the loss of one terminal inositol with phosphate from $[M(Li)_2+Li]^+$. A pair of less abundant fragments observed at m/z 1214 and 1196 represents loss of terminal inositol from $[M(Li)_2+Li]^+$. This spectrum also yielded a less abundant fragment at m/z 1034. The mass difference observed between m/z 1196 and m/z 1034 is 162, which represents the loss of a hexose moiety only. This would be impossible without a rearrangement involving elimination of the

29

Hex residue accompanied by migration of the second phosphate moiety to the charge – retaining Ins•P•Cer moiety. A possible fragmentation pathway would involve formation of an inter-residue cyclic phosphate bridge between Man O-6 and an OH of Ins-1, concomitant with elimination of Ins-2. Elimination of the Man residue could then take place with formation of an intra – residue cyclic phosphate of Ins-1. A proposed structure of such a cyclic phosphate product ion $[PO_3(Li)•Ins•PO_3(Li)•Cer + Li]^+$ is shown in Figure 2-13. From the MS^3 analysis of the m/z 1128 precursor, ceramide related product ions were observed at m/z 718 ($[Cer + Li]^+$) and m/z 786 ($[CerPO_3(Li) + Li]^+$) (Figure 2-11B). The less abundant fragment observed at m/z 966 represents $[Ins•PO_3(Li)•Cer + Li]^+$) indicating the loss of mannose from the m/z 1128 precursor as occurred with MIPC (Figure 2-7 A). A pair of fragments, observed at m/z 417 and 435 in this spectrum, is analogous to the fragments observed in MS^2 analysis of $[M(Li) +Li]^+$ from MIPC, consistent with the residue formula ($[Hex•Ins•P•Li_2]^+$). In MS^4, m/z 718 further fragments to m/z 291 and m/z 324, which is consistent with a t18:0/h26:0 ceramide moiety (Figure 2-11C).

From the m/z 1404 molecular ion, further fragmentation yielded an abundant ion, m/z of 1156 ($[Hex•Ins•P•Li_2]^+$ + $[Cer + Li]^+$) (Figure 2-12A) which again represents the sequential loss of terminal inositol with phosphate from $[M(Li)_2+Li]^+$. All fragments that include Cer are incremented by m/z 28 relative to the m/z 1376 precursor. Thus, fragments representing the loss of a terminal inositol from $[M(Li)_2+Li]^+$ are observed at m/z 1224 and 1242, while the rearrangement leading to formation of the cyclic phosphate product

30

$[PO_3(Li) \cdot Ins \cdot PO_3(Li) \cdot Cer + Li]^+$ is observed at m/z 1062. Products of the m/z

1156 intermediate precursor in MS[3] included ceramide related product ions at

m/z 746 ($[Cer + Li]^+$) and 814 ($[CerPO_3(Li) + Li]^+$) (Figure 2-12B), which also

have an increment of m/z 28 from m/z 718 and 786 respectively. The

$[Ins \cdot PO_3(Li) \cdot Cer + Li]^+$) fragment was observed at m/z 994. In MS[4] analysis m/z

746 further fragments to m/z 319 and m/z 352 (Figure 2-12C), consistent with a

t20:0/h26:0 ceramide moiety. Therefore it was concluded that the predominant

ceramide moieties in $M(IP)_2C$ also have a fatty acyl chain of h26:0 and the

sphingoids comprise a mixture of t18:0 and t20:0 phytosphingosines.
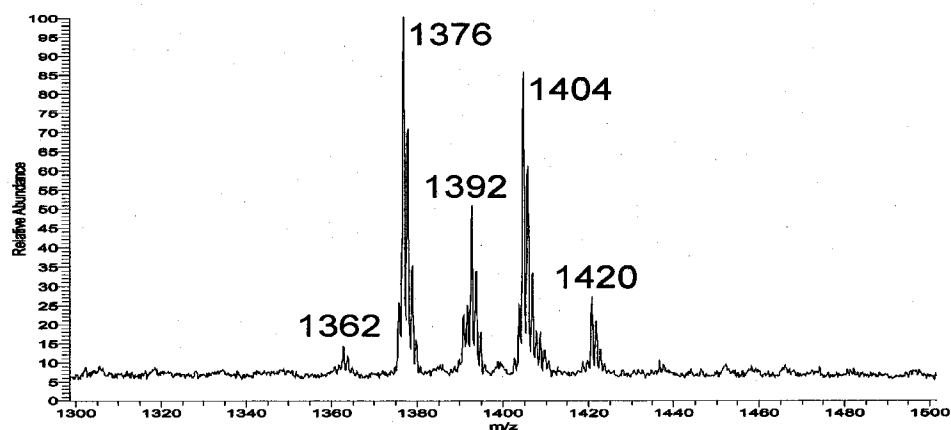
Figure 2-10: ESI-MS[1] Molecular profile of $[M(Li)_2+Li]^+$ adducts for $M(IP)_2C$

31

A
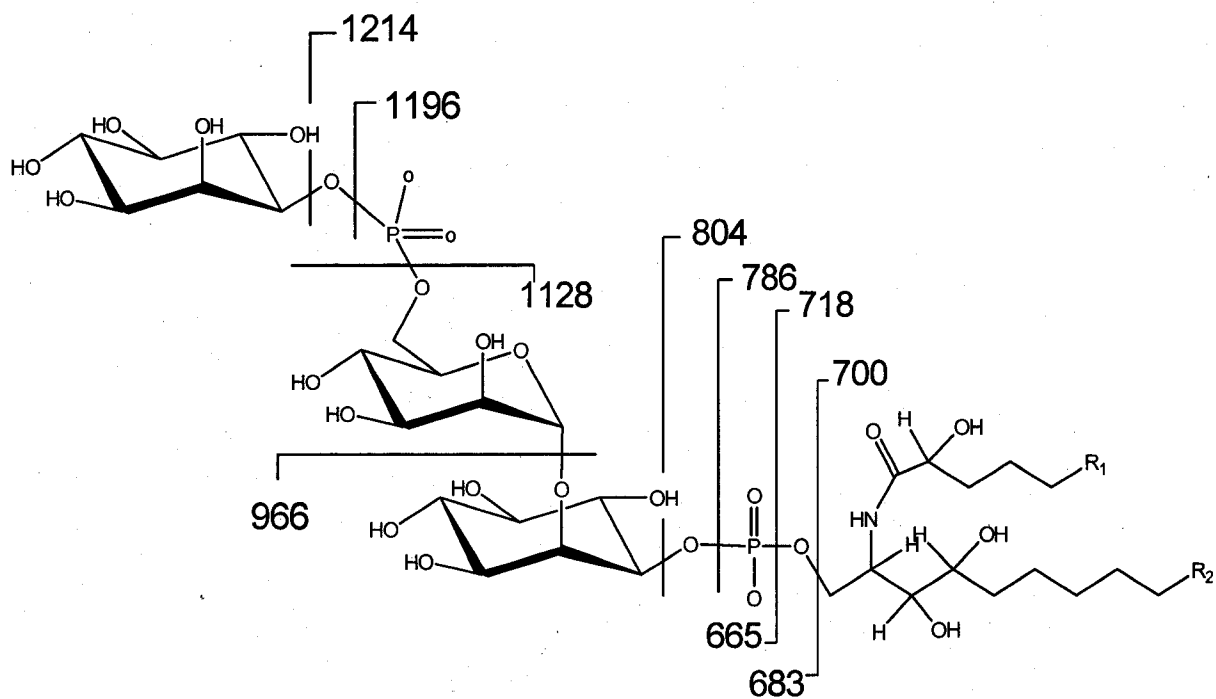
B
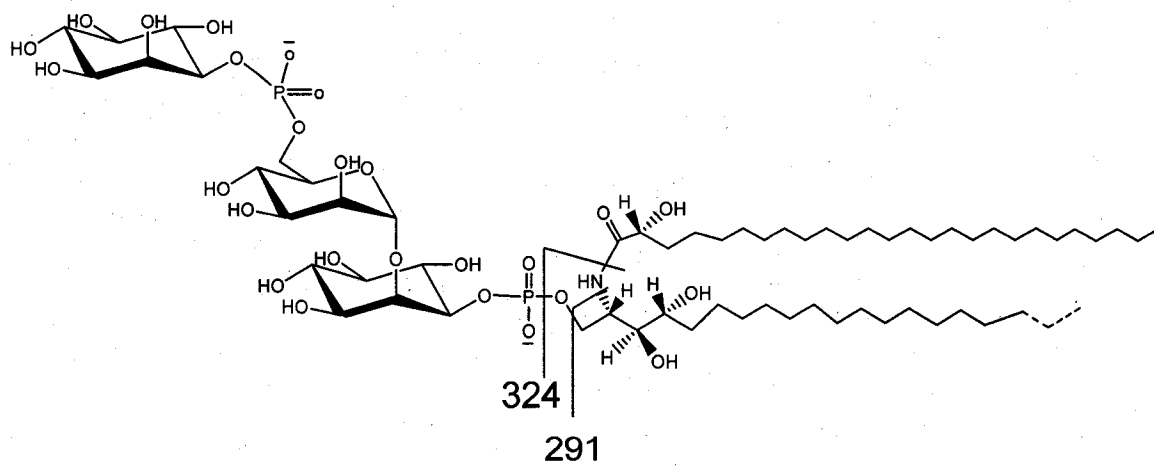
Scheme 2-2: Characteristic fragmentations of the *m/z* 1376 of [M(Li)$_2$+Li]$^+$ adduct of M(IP)$_2$C

32
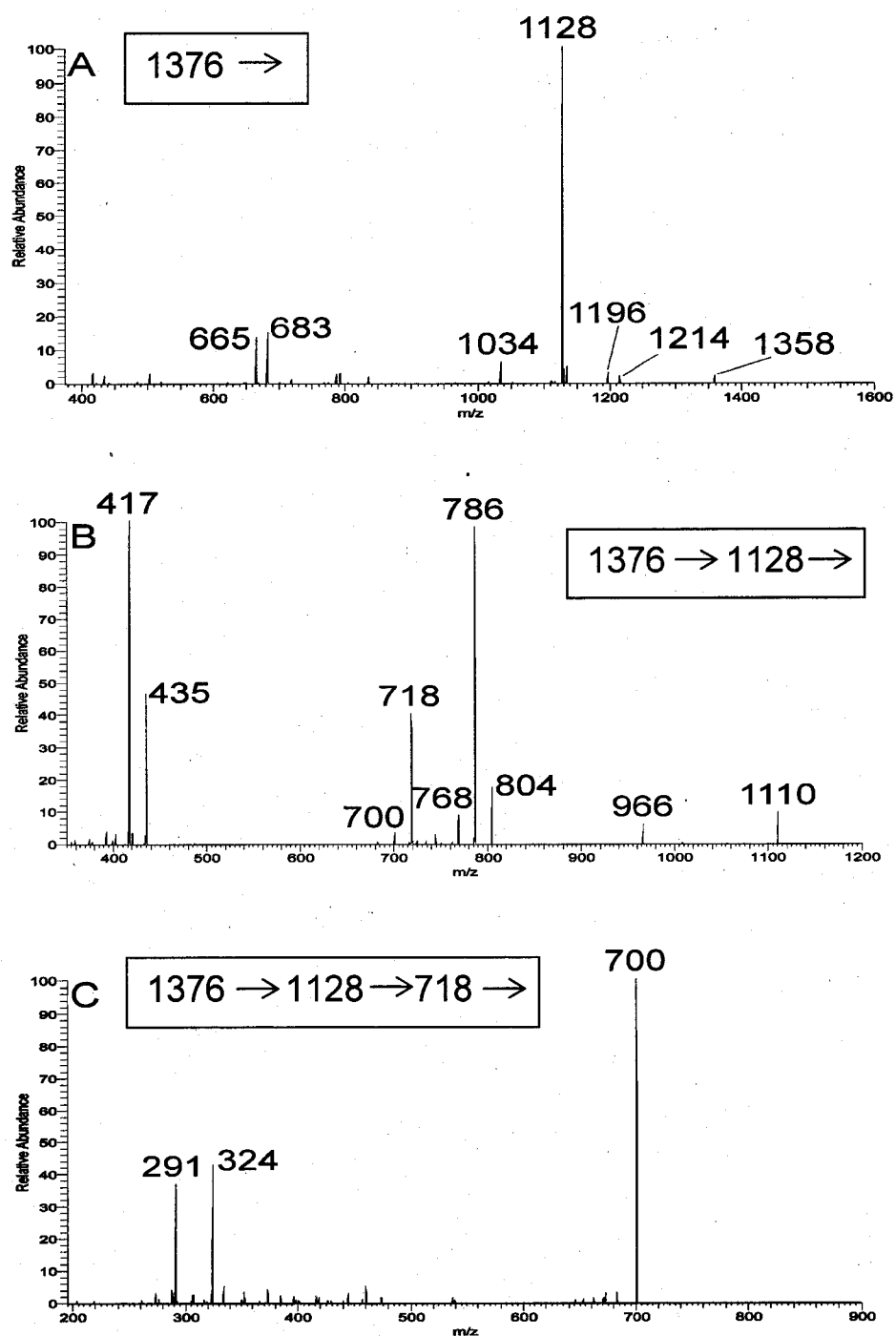
Figure 2-11: MS^2, MS^3, and MS^4 analysis of the [M(Li)$_2$+Li]$^+$ adduct of M(IP)$_2$C *m/z* 1376 (Panels A, B, and C, respectively).
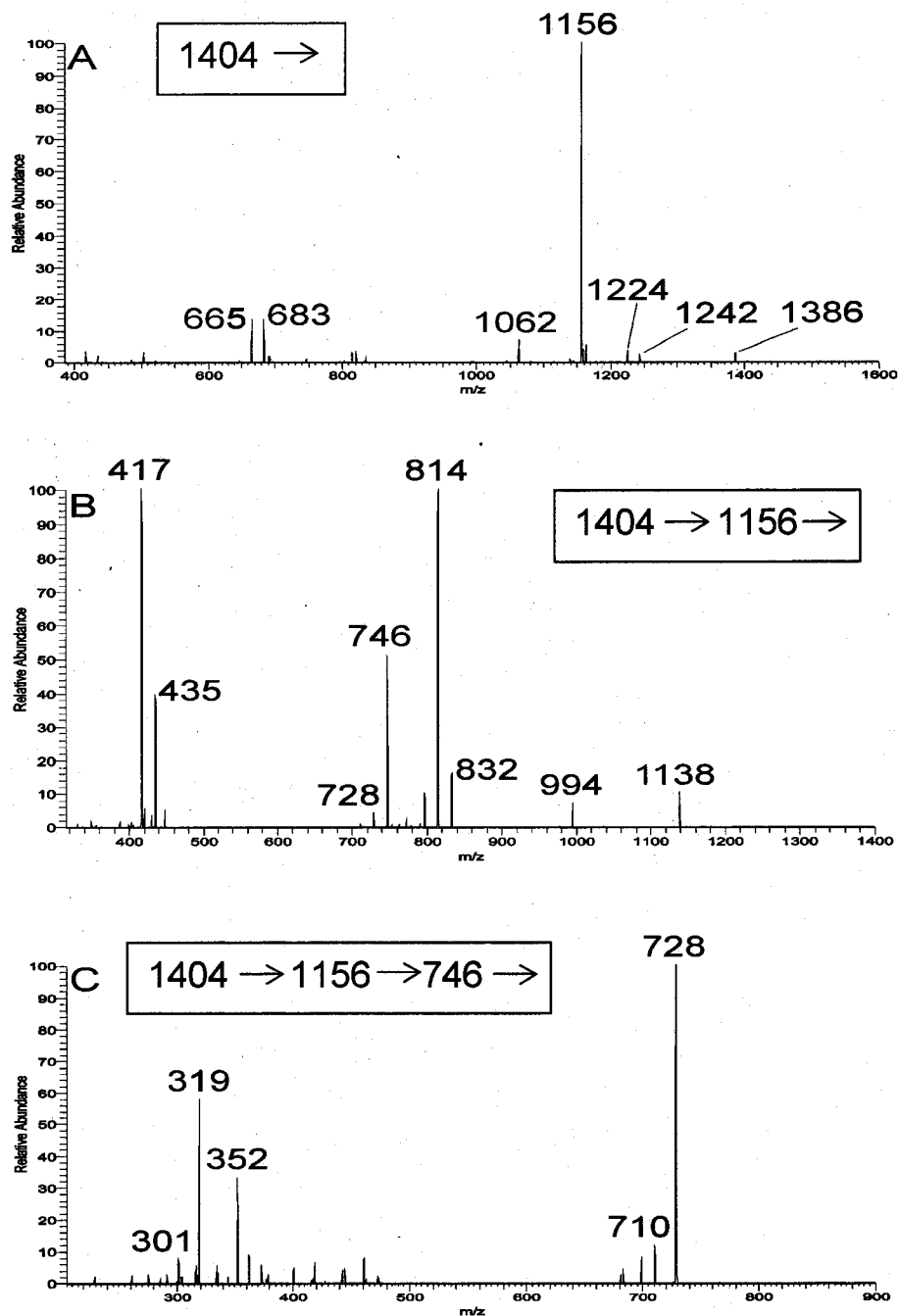
Figure 2-12: MS^2, MS^3, and MS^4 analysis of the [M(Li)$_2$+Li]$^+$ adduct of M(IP)$_2$C m/z 1404 (Panels A, B, and C, respectively).

34
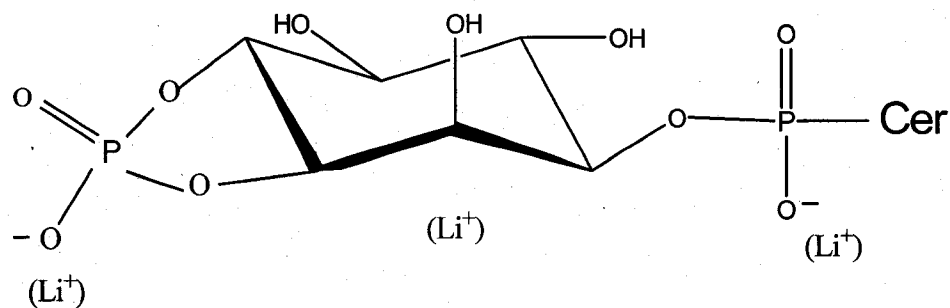
Figure 2-13: Proposed structure of the *m/z* 1034 fragment formed by the migration of the second phosphate group to inositol accompanied by elimination of the Hex residue.

Besides the two major molecular salt adduct peaks at *m/z* 1376 and 1404, other less abundant salt adducts are observed at *m/z* 1392 and 1420, with an increment of *m/z* 16 relative to the two major peaks. The shift of 16 amu is of interest, because it could be consistent with either an additional hydroxyl group on the ceramide or underlithiation, thus corresponding to mixed Na^+/Li^+ salt adducts. A good method to differentiate between these two possibilities is to perform MS^n analysis on these +16 adducts, such as that observed at *m/z* 1392 and compare with the fragmentation profile of *m/z* 1376 parent ion. Figure 2- 14A and B show the MS^3 analysis of the precursors at *m/z* 1392 and 1376 respectively. From the fragmentation pattern, it is clear that a difference of 16 amu is observed between all of the ceramide related ions, which by itself might suggest that there is an extra hydroxyl group attached to the ceramide. However, the 16 amu shift can be observed, at least partially, in the glycosylinositol ions as well. An example is the ($[Hex•Ins•P•Li_2]^+$) ions at *m/z* 435 and 417 from the *m/z*

35

1376 parent ion (Figure 2-14B); these are partially shifted to m/z 451 and 433 when produced from the m/z 1392 parent ion [Figure 2-14A]. Since there is no way for an extra hydroxyl group to be on the glycosylinositol, the 16 amu difference is attributed to underlithiation; that is, the m/z 1392 ion is the $[M(Li)_2+Na]^+$ or $[M(LiNa)+Li]^+$ form of the $[M(Li)_2+Li]^+$ at m/z 1376.
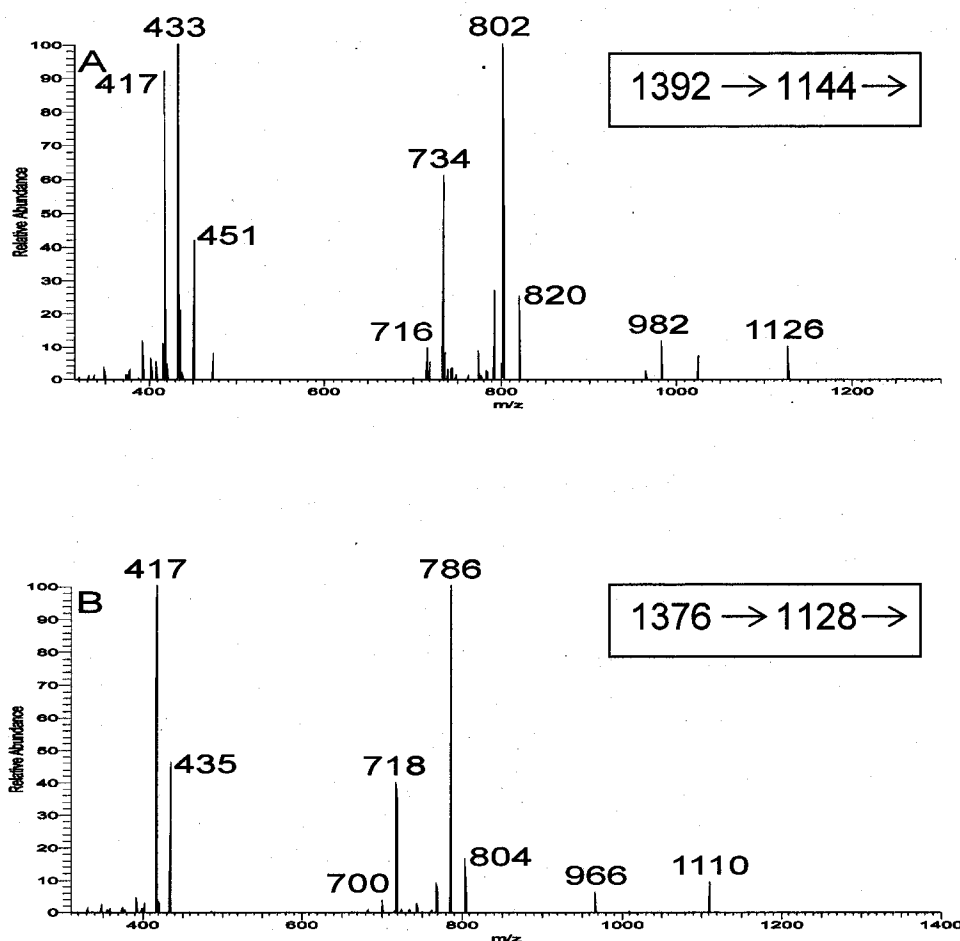
Figure 2-14: MS^3 analysis of M(IP)$_2$C adducts of $[M(Li)_2+Na]^+$ at m/z 1392 and $M(Li)_2+Li]^+$ at m/z 1376.

36

In the MS^2 analysis of m/z 1376 and 1404, a common pair of fragments was observed at m/z 665 and m/z 683. These two fragments were further analyzed to confirm their identity, and found to be consistent with a fragment consisting of one hexose, two inositol, and two phosphate groups. Sequential analysis of these two fragments again confirmed the arrangement of residues in the polar head group of $M(IP)_2C$ as IP-M-IP-C. The MS^n anlysis of m/z 683 is shown in Figures 2-15A and B.
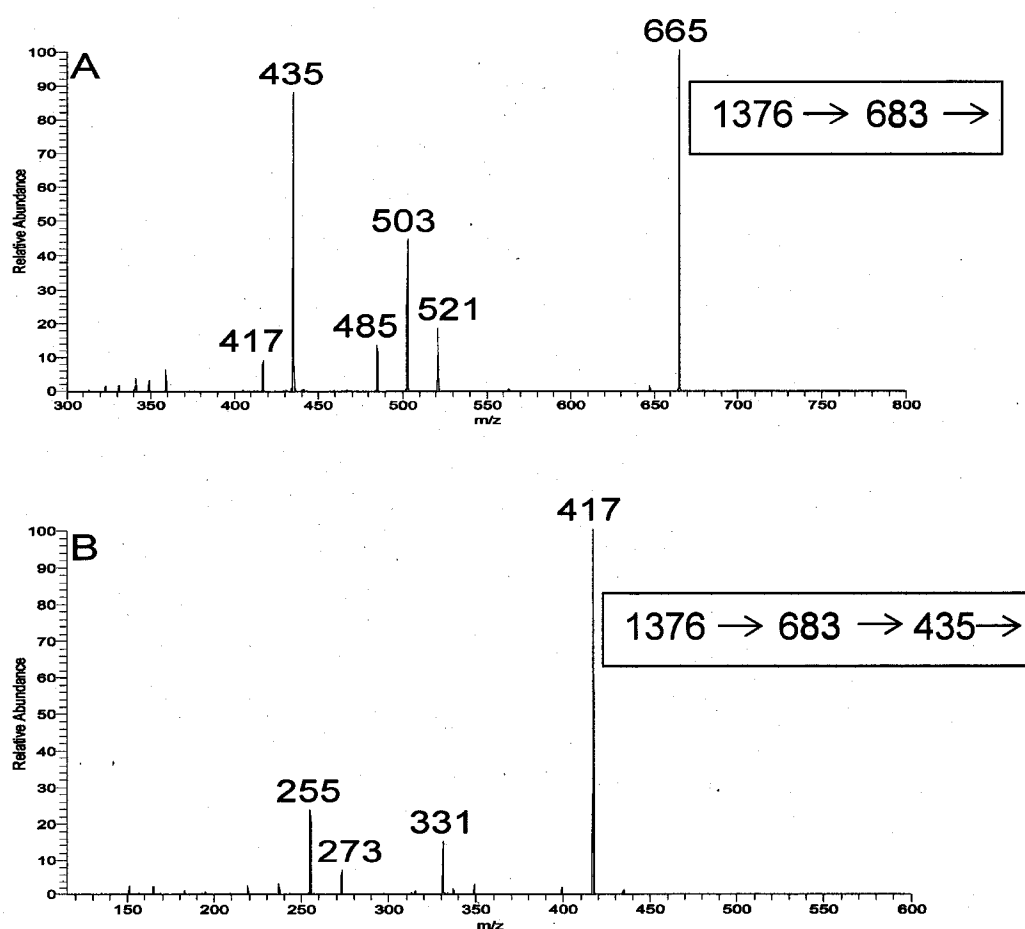
Figure 2-15: MS^3 and MS^4 analysis of the m/z 683 fragment from $M(IP)_2C$ (Panels A and B, respectively).

Fragmentation of *m/z* 683 resulted in a pair of fragments at *m/z* 417 and

435, which are consistent with the residue formula ([Ins•P•Hex•Li$_2$]$^+$), after losing

one inositol with a phosphate group (Figure 2-15A). A pair of fragments

observed at *m/z* 503 and 521 represents loss of inositol without a phosphate

group from *m/z* 683. Further analysis of *m/z* 435 yielded a pair of fragments at

m/z 255 and 273 (Figure 2-15B), following the loss of a hexose, and is consistent

with a residue formula of ([Ins•P•Li$_2$]$^+$). The fragment at *m/z* 331 represents the

non-phosphorylated glycan [Hex•Ins + Li]$^+$. The characteristic fragmentation of

m/z 683 is shown in Scheme 2-3.
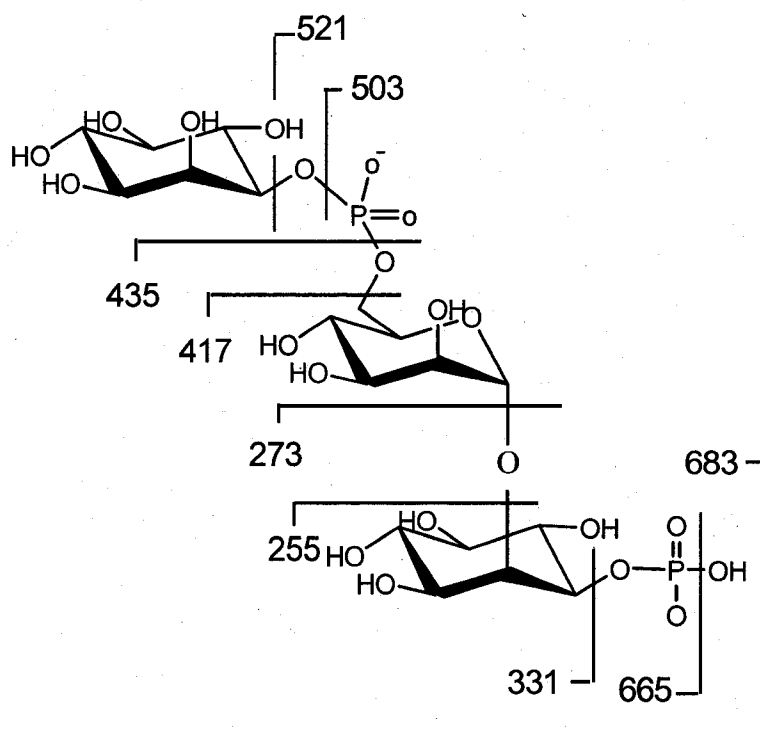
Scheme 2-3: Proposed fragmentation scheme for *m/z* 683 of molecular precursor [M(Li)$_2$+Li]$^+$ at *m/z* 1376

38

Interpretation of the major ions from the MS^n analysis of MIPC and $M(IP)_2C$ is summarized in Table 2-3 and Table 2-4 respectively.

Table 2-3

Interpretation of the major ions from the MS^n analysis of MIPC

m/z	Fragment corresponds to
1128	$[M(Li)+Li]^+$
718	$([Cer + Li])^+$
786	$([CerPO_3(Li) + Li])^+$
291 324	t18:0 phytosphingosine
1156	$[M(Li)_2+Li]^+$
746	$([Cer + Li])^+$
814	$([CerPO_3(Li) + Li])^+$
319 352	t20:0 phytosphingosine

Table 2-4

Interpretation of the major ions from the MS^n analysis of $M(IP)_2C$

m/z	Fragment corresponds to
1376	$[M(Li)_2+Li]^+$
1128	$([Hex \cdot Ins \cdot P \cdot Li_2]^+ + Cer)$
718	$([Cer + Li])^+$
786	$([CerPO_3(Li) + Li])^+$
291 324	t18:0 phytosphingosine
1404	$[M(Li)_2+Li]^+$
1156	$([Hex \cdot Ins \cdot P \cdot Li_2]^+ + Cer)$
746	$([Cer + Li])^+$
814	$([CerPO_3(Li) + Li])^+$
319 352	t20:0 phytosphingosine

39

With respect to glycosylinositol fragmentation, mainly glycosidic cleavages are observed, with possibilities of bond breakage on either side of the glycosidic oxygen, Li^+ retention on either the reducing or the non-reducing portion of the glycan, along with retention or loss of lithium phosphate [30]. The persistence of sets of ions retaining the phosphate provides useful information in structural characterization. The results presented here clearly establish the linkages of the polar groups of MIPC, and $M(IP)_2C$ of *S. cerevisiae* as Manα1$\rightarrow$2Ins1$\leftarrow$P$\rightarrow$1Cer and Ins1$\leftarrow$P$\rightarrow$6Manα1$\rightarrow$2Ins1$\leftarrow$P$\rightarrow$1Cer respectively. It is also evident that the ceramide moieties in MIPC and $M(IP)_2C$ have a fatty acyl chain of h26:0 and the sphingoid is a mixture of t18:0 and t20:0 phytosphingosines. Results in this study could be a preliminary step towards analyzing the possible functional significance of such structures in this or other fungi. In attempts to correlate putative genes with specific glycosyltransferase activities and their possible cellular functions, or to study potential intermolecular interactions of fungal GSLs with host immune system components, precise knowledge of core linkages in fungal GIPCs will be an important consideration.

40

CHAPTER III

INTERACTIONS OF GLYCOSPHINGOLIPIDS WITH PLANT DEFENSINS

Introduction

The basis of the interaction between an antigen and antibody lies in the complimentary shape of each molecule in the vicinity of their binding sites. The highly specific nature of these interactions arises through the contact of the molecular surfaces of antigen and antibody that constitute an epitope and paratope, respectively. Water is generally excluded from the binding sites, and antigen-antibody complexes are stabilized through electrostatic interactions, hydrogen bonding, hydrophobic and Van der Waals forces. Antigen-antibody complexes are among the strongest non-covalent complexes known [47]. The formation of these macromolecular complexes plays an essential role in immune function.

One of the important regulatory roles of glycolipids is activating various signal transduction pathways that control many cellular processes, including immune responses [1]. Foreign GSLs can be recognized as antigens by the immune system. Some GSLs carry mammalian blood group determinants, and they can be strongly immunogenic when associated with foreign proteins or with other cell membrane components. GSLs from fungi, eukaryotic parasites, and sphingosine – synthesizing prokaryotes are also recognized by mammalian host immune systems. A number of glycolipids play a role as tumor- associated

41

antigens and in the immunotherapy of individual cancer forms [36, 37]. Many microbes have selected carbohydrates as a means of colonization and infection on the surface of mammalian cells. Considerable evidence suggests that in most of the cases these binding sites are GSLs, or include GSLs as essential components. Over the past 15-20 years, interest has been sparked by indications that the GSLs play an important role in interactions with plant-derived small antimicrobial peptides called defensins, which target fungal membrane components. The existence of high affinity binding sites for these defensins on fungal plasma membrane fractions has been demonstrated [22].

Plant Defensins

Plants depend on innate immune systems to defend themselves against potentially infectious pathogens that grow epiphytically on their surfaces. No acquired immune system is known for plants, and they lack a circulatory system. However, large repertoires of immune receptors that mediate local responses help trigger systemic defenses, effectively protecting plants from pathogen invasion. In the innate immune response, only one class of peptide seems to be conserved between plants, invertebrates and vertebrates, namely defensins. Defensins are small (45-54 amino acids) highly basic, cysteine-rich peptides expressed in species from all eukaryotic kingdoms including insects and humans [22, 24]. Up to now, three types of defensins have been identified in mammals; α- and β- defensins, which occur generally, and θ-defensins, which have only been discovered in macaques. The plant defensin family is quite diverse regarding amino acid composition, but all plant defensins identified so far have eight

42

cysteines that form four structure-stabilizing disulfide bridges. Based on the overall three-dimensional structure, there is a closer relationship between plant defensins, insect defensins and mammalian β-defensins than between mammalian α- and β- defensins [22]. This suggests that defensins are ancient peptides conserved across the eukaryotic kingdom, originating before the evolutionary divergence of plants and animals. Possibly, defensins have evolved from a single precursor, being a molecule with an overall structure resembling that of plant defensins. Three-dimensional structures of defensins of various origins and the amino acid sequences of a mature plant defensins, RsAFP1 and RsAFP2, from radish seed are shown in Figure 3-1A and B respectively.
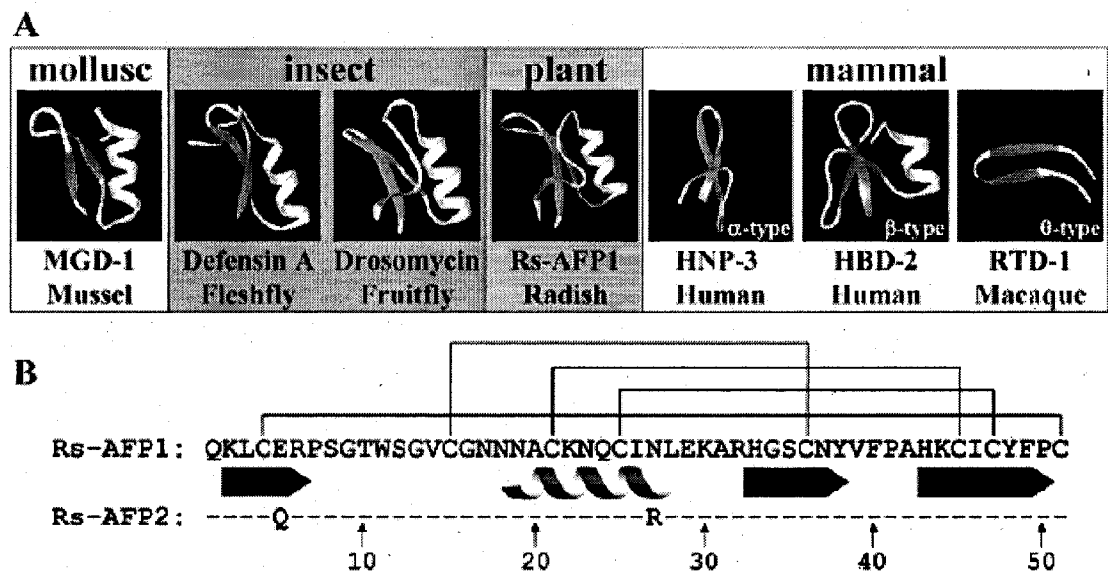
Figure 3-1: A. Three-dimensional structures of defensins of plant, invertebrate (insect and mollusc) and vertebrate (mammalian) origin. Structures were downloaded from the protein data bank (http://www.rcsb.org/pdb. B. Amino acid sequence of mature Rs-AFP1 and 2. Dashes indicate identical amino acid residues. Connecting lines between cysteine residues represent disulfide bonds and the spiral and arrows indicate the location of α- helix and β strands, respectively.

43

Most plant defensins isolated to date exhibit antimicrobial activity, and several have strong antifungal activity against a broad range of species. Structural determinants in plant defensins that govern their antifungal activity, and the mechanisms by which they inhibit fungal growth, remain unclear. A number of studies have attempted to unravel the mode of action of plant defensins. Based on the available evidence researchers have proposed a two-step model. This model suggests that the first step in the path leading to fungal growth inhibition would be binding of the plant defensins to specific sites on the plasma membrane of fungal hyphae. Interaction with these binding sites subsequently would enable plant defensins to insert into the plasma membrane, thus affecting membrane structure and permeability to certain solutes, such as Ca^{2+} and K^+, some of which play an important role in fungal growth and development. This theory also suggests that once into the interior of the cell, the defensins affect protein synthesis and target other cytoplasmic components like RNA and DNA [24, 25]. These effects combined or alone would lead to fungal growth inhibition and cell death. It has been shown that GSLs are the specific binding sites for plant defensins in the fungal cell membrane, in some cases $M(IP)_2C$, and in others GlcCer [26].

Interestingly, several plant defensins are active against human fungal pathogens such as *C. albicans* [29, 30]. So far, none of the plant defensins has been found to cause detrimental effects on cultured human or plant cells. Several experiments point towards a role of defensins in defending the host from fungal attack [25]. The selective activity of plant defensins against fungal cells is most

44

likely a result of differences at the level of the plasma membrane between fungi and plant cells. It has been shown, however, that some interact specifically with GSLs in the fungal cell membrane. Structural differences in these membrane components between fungal and plant cells may in part account for the non-toxic properties of plant defensins for plant cells.

Fungal GlcCer show a number of structural features that distinguish them from those found in mammals and plants. In most fungal species, GlcCer is composed primarily of a 9-methyl-4,8-sphingadienine which is linked to a C16 or C18 α-hydroxy fatty acid [35]. GlcCer of mammalian origin usually have nonhydroxylated fatty acids. While the fatty acid in yeast GlcCer is mostly saturated, the fatty acids in GlcCer from filamentous fungi can be Δ^3 – unsaturated to varying extents, with the proportion of unsaturation depending on species, strain, morphology, and culture conditions [32]. In plants, GlcCer structures are diverse. So far the main difference between fungal and plant GlcCer appears to be the addition of a branching 9-methyl group to the fungal sphingadienine base and complete lack of Δ^3 – unsaturation in the plant fatty acid moiety [35]. The effects of these structural differences in binding specificity will be discussed in detail later in this chapter.

This chapter of the thesis describes experiments performed to study the possible interactions of fungal GSLs with plant defensins. Although it was originally intended to study the putative interactions of M(IP)$_2$C with a defensin from radish (RsAFP1 or RsAFP2) these have recently become unavailable. Therefore, another model system has been used, employing a defensin (MsDef1)

45

from alfalfa *(Medicago sativa)*, which has been proposed to interact with GlcCer

from the fungus *Fusarium graminearum,* the agent of head blight disease in

cereals [38, 39]. GlcCer variants from the crude neutral lipids of several fungi

whose structures have been established previously [32, 33, 34, 35] as identical to

that of *F. graminearum,* or contain known structural variations, were obtained and

purified. These were employed in interaction studies with MsDef1. GlcCer of

plant origin (extracted and purified from soy beans) and mammalian GlcCer and

GalCer were used as further controls in these studies. The purpose here was to

determine the potential significance of structural variations of both sugars and

ceramides, in order to elucidate the specificity and sites of binding interaction. In

this project a number of different experimental approaches were used to study

the potential interactions of GSLs with plant defensins. Two traditional

immunochemistry methods (TLC immunostaining and ELISA assays) were

employed, and the results are discussed. A preliminary attempt to detect an

MsDef1 – GlcCer complex by mass spectrometry was also carried out. There are

many precedents for characterization of non-covalent complexes by mass

spectrometry, but this is still controversial, and it is a challenge to prove

specificity [47]. The main challenge is to ionize and transfer potentially fragile

complexes from solution or solid into the gas phase, and particular attention has

to be paid to understand and control the variety of processes involved. Matrix –

assisted laser desorption ionization (MALDI) MS of proteins produces

predominantly singly charged ions, which are within the normal range of

detection of the time-of-flight (TOF) analyzer. However, the energies used for

46

desorption may be unsuitable for maintaining a non-covalent complex. In contrast, the energies used in electrospray ionization (ESI) are much lower. Proteins and their complexes are generally larger than the normal mass range of the analyzers employed, but ESI-MS produces multiply charged ions, thereby bringing large molecular ions in to the *m/z* range of commercial mass spectrometers that are not able to detect their singly charged counterparts. Attempts to use both types of MS modes are described in this chapter.

Experimental Methods

Solvents for extraction, high performance thin layer chromatography, silica gel and Iatro beads column chromatography.

All solvents used were of highest grade available (HPLC grade). Milli-Q water was used for solvent preparation. Solvent A, chloroform/methanol (1:1 v/v); Solvent B, isopropanol/hexane/water (55:25:20 v/v); Solvent C, chloroform/methanol/water (30:60:8 v/v/v); Solvent D, isopropanol/hexane/water (55:40:5 v/v/v); Solvent E, chloroform/methanol/water (60:35:8 v/v/v); Solvent F, chloroform/methanol (95:5 v/v); Solvent G, chloroform/methanol (9:1 v/v); Solvent H, chloroform methanol (8:2 v/v).

Extraction and fractionation of neutral glycosphingolipids

Fungal growth and isolation were performed according to the standard protocol available in the laboratory. Extraction and purification of glycosphingolipids were carried out as described previously with some modifications and additional steps [34, 35]. Briefly, GSLs were extracted by

47

homogenizing mycelia (25-35 g) in a glass walled blender, once with 200 mL of solvent A, two times with 200 mL of solvent B and once more with 200 mL of solvent A. The four extracts were pooled and dried on a rotary evaporator at 40 °C. The dried residue was partitioned between water and 1-butanol pre-saturated with water (200 mL each) with vigorous shaking in a separatory funnel. The lower (water) layer was discarded, and similarly extracted 3 more times with equal volumes of water-saturated 1-butanol. The four 1-butanol extracts were combined in a round-bottom flask and evaporated to dryness. These samples were then transferred to 16x100 screw cap test tubes, conserving all material and treated with 20 mL methanol-water-1-butanol (4:3:1 v/v/v) containing 25-30% methylamine at 55 °C for 4 hours on a rocking platform. The lipids were dried under N_2 stream at 35-40 °C and re-suspended in solvent C. The crude lipids were separated in to neutral and acidic fractions using a DEAE-Sephadex A-25 (weak anion exchanger) column. Neutral lipids were eluted with five bed volumes of solvent C, dried and taken up in 1 mL of solvent D. High performance thin layer chromatography (HPTLC) was then performed on the neutral fraction.

High Performance Thin Layer Chromatography (HPTLC)

TLC analysis was performed on silica gel 60 pre-coated HPTLC plates (E.Merck, Darmstadt, Germany). The crude lipid samples dissolved in solvent D were applied to the plate by streaking from 10 µL microcaps. Analytical TLC was performed using solvent E as the mobile phase. Detection was made by Bial's orcinol reagent (orcinol 0.55% [w/v] and H_2SO_4 5.5% [v/v] in ethanol/water

48

9:1[v/v]; the plate is sprayed and heated briefly to 200-250 °C; violet/purple staining is positive for the presence of hexose).

Column Chromatography (silica gel-60)

Glucosylceramides from the crude lipids were separated by column chromatography using silica gel (Merck, 70-230 mesh, 60 Å) as the stationary phase. A 2 x 25 cm glass column, with a 250 mL solvent reservoir, was packed with silica gel slurry prepared in a 95:5 v/v chloroform/methanol solvent mixture. The crude lipid sample was applied to the column and five bed volumes each of three solvent systems (F, G, and H) were used as mobile phase.

Column Chromatography (Iatro beads)

Glucosylceramides partially separated by the silica gel column were further purified by column chromatography using Iatro beads (6RS-8010; Iatron Chemical Laboratory, Tokyo, Japan) as stationary phase. A 2 x 25 cm glass column, with 250 mL solvent reservoir, was packed with a slurry of Iatrobeads prepared in a 95:5 v/v chloroform/methanol solvent mixtures. The lipid fraction eluted with solvent G from the silica gel column (lane 2 of silica gel column profile) was loaded onto the Iatro beads column and five bed volumes each of four mobile phase solvent systems (100% chloroform, solvents F, G, and H) were used.

TLC- overlay staining with anti-GlcCer

Glycolipids were spotted on silica-60 TLC plates with plastic support (two identical sets) and developed with a solvent system of chloroform: methanol: water (60:35:8, v/v/v). One set was visualized by spraying with orcinol and

49

heating to 200-250 °C. For immunostaining, the region of the plate where GSLs are located was cut as a strip comparing with the visualized duplicate, so that the spots would correspond in position to those on the orcinol stained duplicate. This strip was incubated with blocking buffer (1% polyvinylpyrrolidone and 0.1% nonfat dry milk in 50mM Tris-HCl, pH 7.4, 200 mM NaCl) for 1 hour at room temperature. After removing the excess blocking buffer, the plate was incubated with rabbit antiserum against GlcCer (GlycoTech, Germany) at a dilution of 1:200 (in blocking buffer) overnight at room temperature. After five washings (5 min each with 20 mL) in washing buffer (50 mM Tris-HCl, pH 7.4, 200 mM NaCl), the plate was incubated with peroxidase – conjugated goat anti-rabbit immunoglobulin(Ig)G (purchased from Dianova, Hamburg, Germany) diluted 1:1000 in blocking buffer for 2 hours at room temperature. The plate was washed four times as before, and a fifth time in the substrate buffer (0.1 M sodium citrate, pH 4.5). Bound antibody was then detected by incubation with substrate solution (10 mL) which was freshly prepared and composed of 8.33mL substrate buffer, 1.67 mL of 4-chloro-1-naphthol (3mg/mL in methanol) and hydrogen peroxide (3.5 µL of a 30% solution).

TLC- overlay with plant defensin (MsDef1)

Above described procedure was followed with few modifications. The initial steps were carried out without any significant changes. After the removal of excess blocking buffer, the plate was incubated with plant defensin (MsDef1, 85 µM) at a dilution of 1:10(in blocking buffer), overnight at room temperature. As before, after five washings in washing buffer, the plate was incubated with anti-

MsDef1 antibody (200 µM) diluted 1:100 in blocking buffer for 2 hours at room temperature. The plate was then washed and incubated with peroxidase – conjugated goat anti-rabbit immunoglobulin (Ig) G diluted 1:1000 in blocking buffer for 2 hours at room temperature and detected by incubation with freshly prepared substrate solution.

<u>Enzyme-Linked ImmunoSorbent Assay (ELISA)</u>

PolySorp 96-well microtiter plates (Nalge Nunc International, Denmark) were used for the assay. Different GSLs were dissolved and serially diluted in methanol. Approximately 1 µg of GSL was used in the first well of each ELISA assay. Wells of the plate were coated with GSLs in methanol and dried under a hood. Unless stated otherwise 50 µL volumes were used. Any non specific binding sites on the wells were blocked with 200 µL of 10 mM phosphate buffered saline (PBS) supplemented with 1% bovine serum albumin (BSA) for 2 hours at room temperature. Two different antifungal plant defensins were used for the study; MsDef1 and MtDef4. After removing excess blocking solution by inverting the plate on paper towels, the wells were incubated with appropriate dilutions of plant defensins in blocking solution (MsDef1, 85 µM, diluted to 1:10 and MtDef4, 200 µM, diluted to 1:20) overnight at 4 °C. After 3 washings in PBS (10mM) the wells were incubated with the appropriate anti-defensin antibody diluted in blocking solution for 2 hours at room temperature. The plate was washed 3 times in PBS (10mM) and peroxidase – conjugated goat anti-rabbit immunoglobulin(Ig)G (purchased from Dianova, Hamburg, Germany) diluted 1:1000 in blocking buffer was added and incubation was continued for 2 hours at

51

room temperature. After the plate was washed in PBS (3 times), the plate was incubated with freshly prepared substrate solution, which was composed of 1mg azino-di-3-ethylbenzthiazolinsufonic acid (ABTS salt) dissolved in 1mL substrate buffer (0.1 M sodium citrate, pH 4.5) with sonication in an ultrasound water bath for 3 min followed by the addition of hydrogen peroxide (2.5 µL of a 30% solution). After 30 min at 37 °C on a rocking platform, the reaction was stopped by the addition of 2% aqueous oxalic acid and the plates were read by a microplate reader (Bio-Tek Instruments, Inc. VT, USA) at 405 nm.

MALDI-TOF MS Analysis

MALDI- TOF mass spectrometry was performed on a Shimadzu Axima – CFR (Manchester, England). The matrix was prepared by dissolving 10 mg α-cyano-4-hydroxy cinnamic acid (CHCA) in 1mL acetonitrile: water (50:50 v/v). For the analysis of GSLs, the matrix was spotted on the MALDI target (1 µL), followed by a 1 µL spot of sample dissolved in methanol, and allowed to dry before analysis. For the analysis of defensins (MsDef1), 0.5 µL of the sample in buffer was mixed with 1.5 µL of matrix and an aliquot of this mixture (1 µL) was spotted on the MALDI target and allowed to dry before analysis. All samples were analyzed in positive ion mode using the reflector detection mode.

ESI-MS Analysis

Electrospray ionization mass spectrometry was performed on a Finnigan LTQ equipped with an Advion Triversa Nanomate ESI chip. GSLs dissolved in methanol and defensins in buffer were analyzed in the positive ion mode with a spray voltage of 1.4 kV.

Immunochemistry for the MS analysis

Formation of MsDef1-GSL complex for MS analysis was attempted by allowing a 1:1 mixture of MsDef1 (in buffer) and GSL (in methanol) to stand for a period of 2 h at room temperature. For MALDI-MS analysis, the matrix was spotted on the MALDI target (1 µL), followed by a 1 µL spot of the reaction mixture and allowed to dry before analysis. For ESI-MS analysis, 5 µL of the mixture was placed in one well of the 96-well sample plate of the Nanomate ESI chip.

Results and Discussion

After treatment with a strong base and fractionation by anion exchange, profiles of crude neutral lipids were compared by HPTLC analysis. Figure 3-2 shows the TLC profile of crude neutral lipids from the mushroom *A. bisporus*. Previously characterized GlcCer from *S. schenckii* and *C. neoformans*, respectively, were used for comparison (represented in lanes S). Lanes 1 and 2 shows the presence of glucosylceramides in the crude samples.
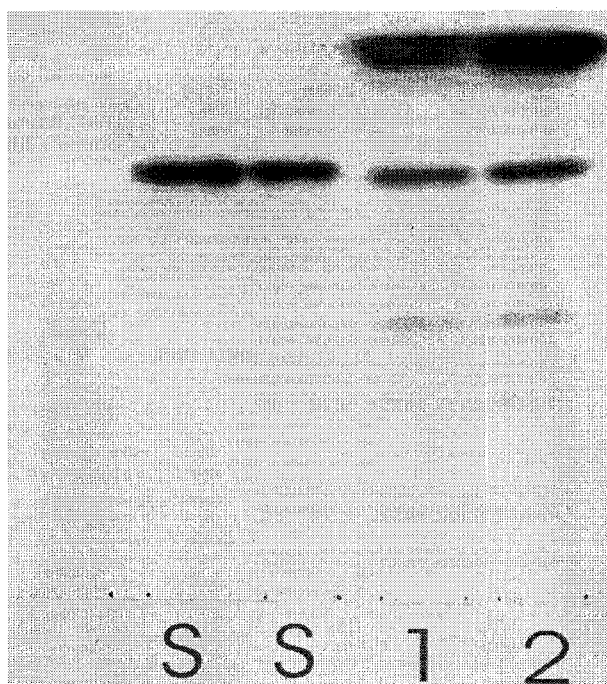
Figure 3-2: TLC profile of crude neutral lipid sample fractions detected using orcinol. Lanes S = two different GlcCer standards from *S. schenckii* and *C. neoformans,* respectively, Lanes 1and 2 = crude neutral lipids (two different batches) from *A. bisporus.*

The purity of GSL samples is very important in binding assay experiments. Impurities in the samples can undergo non specific interactions with antibodies and give ambiguous results, which could be misleading. To obtain pure GlcCer, crude lipid fractions were subjected to purification by column chromatography using silica gel as the stationary phase. Figure 3-3 shows the TLC profile (orcinol stain) of glucosylceramide fractions from the mushroom *A. bisporus* separated using silica gel as the stationary phase. Lanes 1, 2 and 3 represent consecutive fractions eluted by mobile phase solvents F, G, and H, respectively. Glucosylceramides along with some impurities, were eluted with solvent G (lane 2).
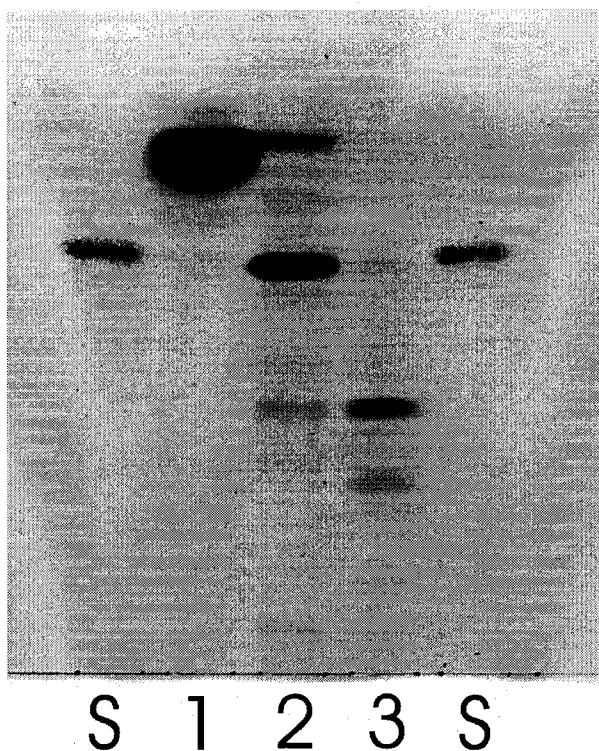
54

Figure 3-3: TLC analysis of neutral glucosylceramide fractions separated using silica gel column chromatography (detected using orcinol). Lanes S = two different GlcCer standards from *S. schenckii* and *C. neoformans*, respectively, Lane 1= fraction collected in solvent F, Lane 2 = fraction collected in solvent G, Lane 3 = fraction collected in solvent H.

Further purification of the solvent G eluted fraction was achieved by column chromatography using Iatrobeads as the stationary phase (these are spherical silica gel particles with exceptional uniformity with respect to particle and pore size). The same mobile phase solvent systems (F, G, and H) used with the silica gel column were employed in Iatrobeads chromatography. TLC analysis of the separated fractions (Figure 3-4) showed that the fraction eluted with solvent G (lane 3) now contained pure GlcCer.
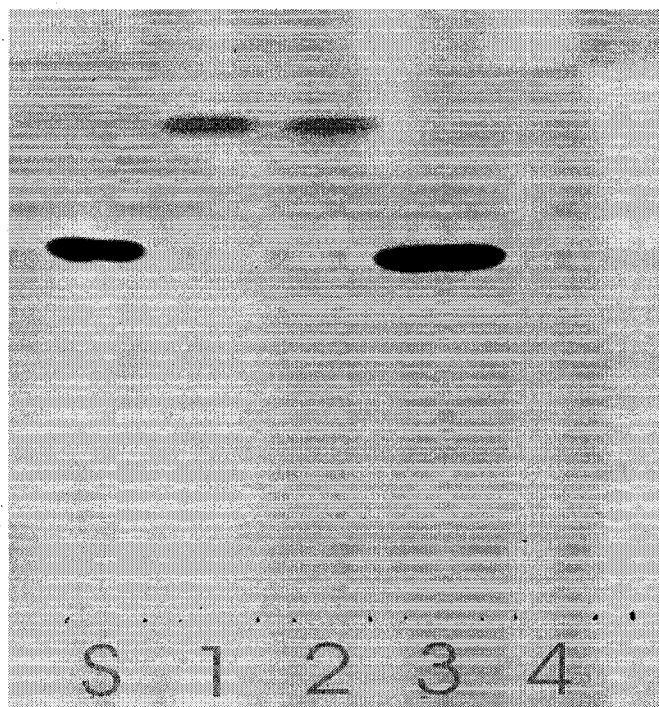
55

Figure 3-4: TLC analysis of the neutral lipid fraction eluted by solvent G, following second chromatography on latrobeads column (detected using orcinol). Lane S = GlcCer standard, Lane 1 = fraction collected in 100% $CHCl_3$, Lane 2= fraction collected in solvent F, Lane 3 = fraction collected in solvent G, Lane 4 = fraction collected in solvent H. Glucosylceramides were eluted with solvent G (lane 3).

Essentially identical protocols were used to purify mono-hexosyl ceramides fractions from crude neutral lipids of two other fungal species, *Aspergillus fumigatus* and *Neurospora crassa*. TLC analysis of purified neutral GlcCer fractions from these two fungi, purified using sequential silica gel and latrobeads column chromatographies is shown in Figure 3-5A and B.
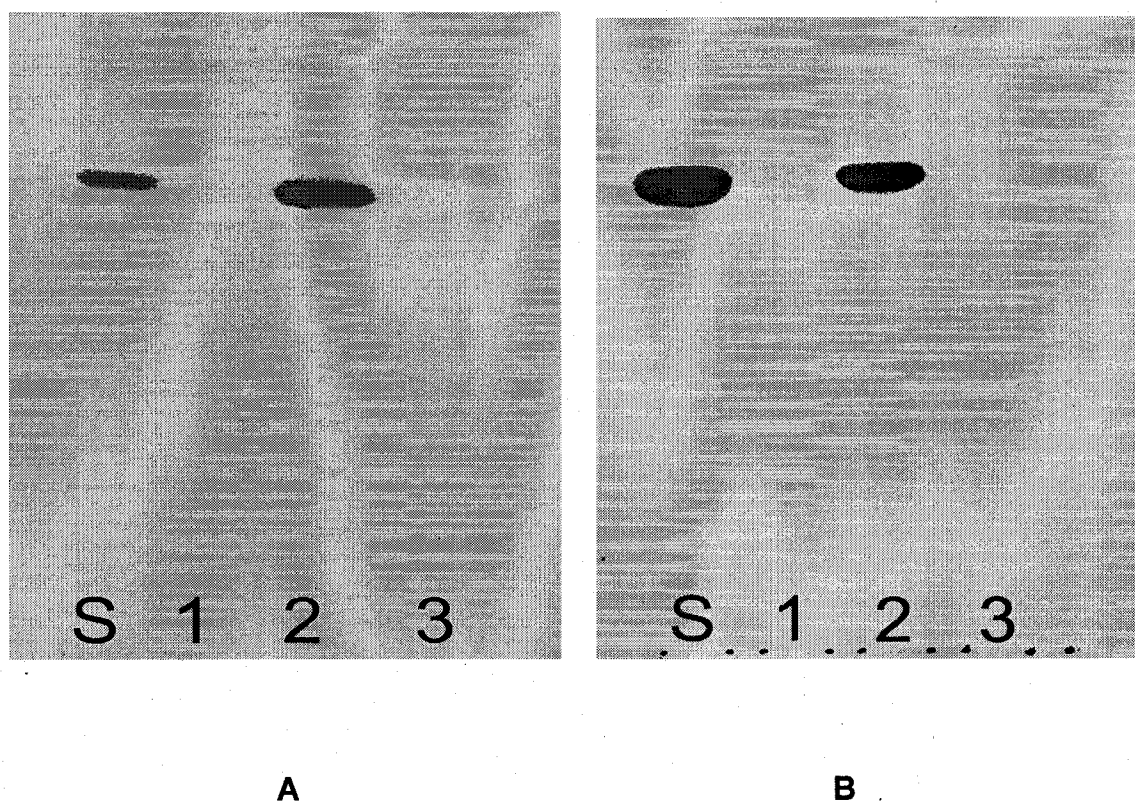
56

A   B

Figure 3-5: TLC profile of neutral glucosylceramide fractions from *A. fumigatus* (A) and *N. crassa* (B) subjected to sequential silica gel and Iatrobeads column chromatography detected using orcinol. Lane S represents the GlcCer standard used for comparison. Lanes 1, 2, and 3 represent the fractions eluted from Iatrobeads with mobile phase solvent systems F, G, and H, respectively. Glucosylceramides were eluted with solvent G (lane 2).

Previously isolated and purified glucosylceramides of various origins

were obtained for use as controls with different or identical structural features in

the binding assay experiments. These are GlcCer from another fungal species *F.*

graminearum; and GlcCer of plant origin (extracted from soy beans); GlcCer and

GalCer of mammalian origin. TLC analysis of all GSLs used in the binding assay

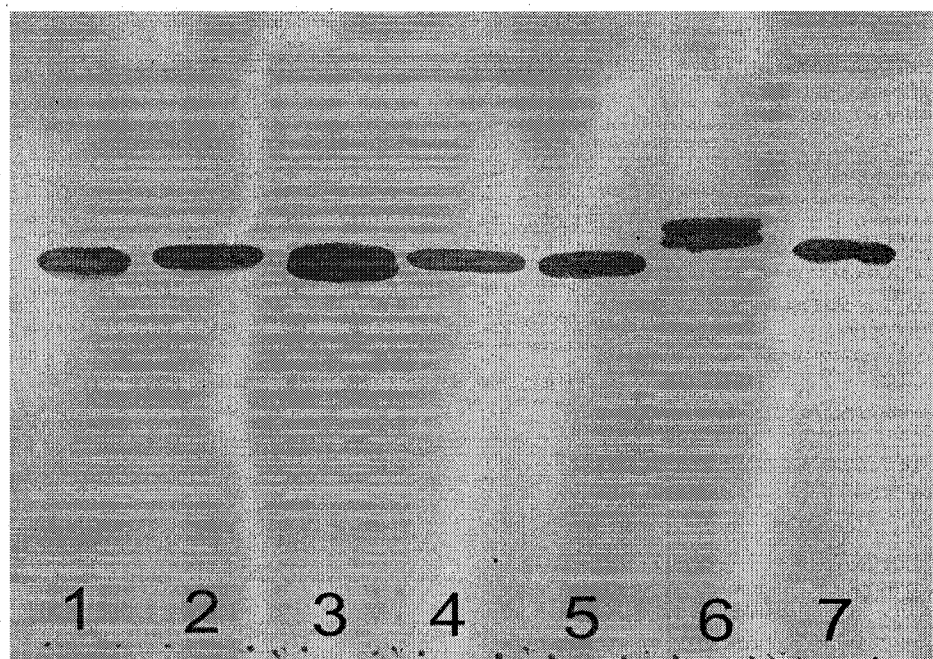experiments is shown in Figure 3-6.

57

Figure 3-6: TLC analysis of purified neutral monohexosylceramides of various origins.

Lane 1 – *A.bisporus*   -GlcCer
Lane 2 – *A.fumigatus*   -GlcCer
Lane 3 – *N.crassa*   -GlcCer
Lane 4 – *F.graminearum*   -GlcCer
Lane 5 – Soybean   -GlcCer
Lane 6 – Human   -GlcCer
Lane 7 – Bovine brain   -GalCer

Identities and purities of all GSLs used in the study were confirmed using

MALDI -TOF-MS (spectra shown in Appendix B).

TLC overlay staining with anti-GlcCer

This study was planned as a preliminary step before investigating the

specific binding of plant defensins to GSLs by TLC immunostaining. The purpose

of this step was to gain practical knowledge about experimental conditions for

binding a protein to immobilized GSLs, i.e.,to establish my ability to use

58

antibodies against glycolipid antigens in a TLC overlay protocol. In this experiment a commercial polyclonal antiserum raised against GlcCer of plant origin or human origin, was tested against GlcCer from two different fungi and a mammalian GlcCer. TLC images visualized by orcinol and by immunostaining are shown in Figure 3-7A and B respectively. It was found that the antiserum bound to both of the fungal GlcCer, but showed little detectable binding to mammalian GlcCer.

A   **B**

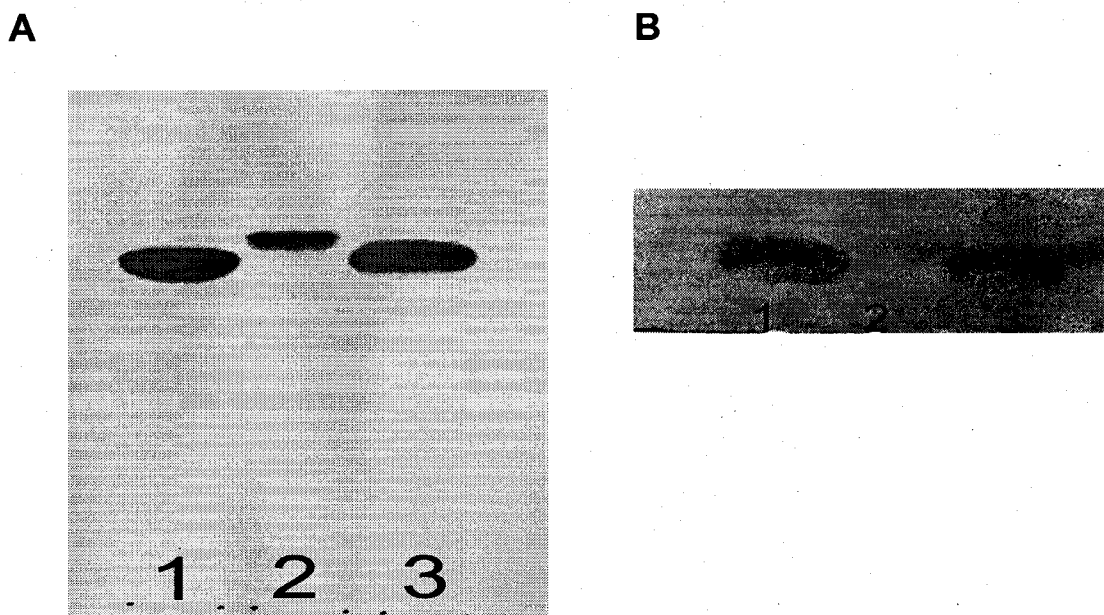Figure 3-7: TLC images visualized by orcinol (A) and by immunostaining (B). Lanes 1 and 3 represents GlcCer from *A.bisporus* and *A.fumigatus* respectively. Lane 2 represents GlcCer from Mammalian origin.

TLC overlay staining with plant defensin (MsDef1)

These experiments employed a defensin MsDef1 from alfalfa (*Medicago sativa*) which has been shown to have antifungal activity [26]; attempts were

59

made to develop an overlay protocol for MsDef1 binding using two different fungal GlcCer along with mammalian GlcCer on the TLC plate. Various experimental conditions were tested in order to observe binding. However, this experiment did not give any interpretable results. Regardless of the different experimental conditions tried, the defensins appeared to have a nonspecific interaction with the silica gel surface of the plate. When the plate was stained with the detection antibody and substrate, a dark blue color developed evenly on the entire surface of the plate, no matter what GSLs were spotted on it, or where the spots were located, and even when no glycolipid was spotted at all. On the other hand, when primary antibody, secondary antibody, or MsDef1 was left out on the protocol, there was no staining at all. We speculate that defensins, which are highly basic in nature, might have a high affinity for the acidic sites on the silica, and are not removed from the silica surface by normal washing steps, which leads to uniform darkening of the plate. Development of an overlay protocol for MsDef1 binding was therefore abandoned.

Enzyme-Linked ImmunoSorbent Assay (ELISA)

The binding specificity of MsDef1 was further analyzed by an ELISA assay which should be sensitive in detecting specific antigen-antibody type interactions, and does not use an acidic solid surface. GlcCer from four different fungal species and plant GlcCer, along with GlcCer and GalCer from mammalian origin, were analyzed in the initial experiment (Figure 3-8). Structures of all GlcCer employed in this study are shown in Figure 3-9 and 3-10. In this assay, all fungal and plant GlcCer showed specific binding to MsDef1 in a concentration

60

dependent manner. No reactivity was observed with mammalian GlcCer and GalCer at any concentrations.
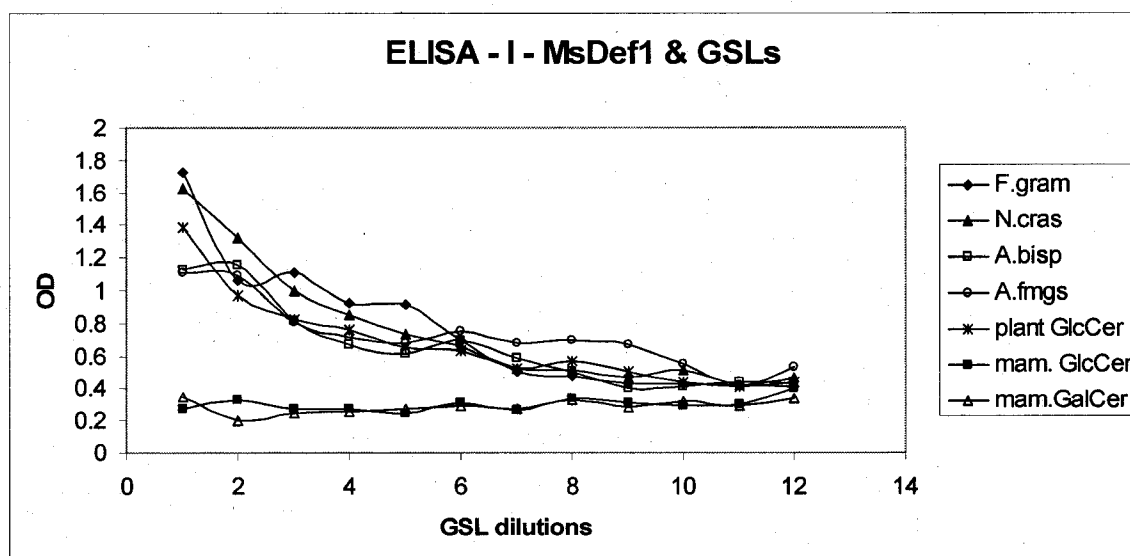
ELISA - I - MsDef1 & GSLs

Figure 3-8: Binding curves showing reactivity of MsDef1 with varying concentrations of GSLs.

Structural details of the GSLs used in the experiment were compared to understand their differences and to shed light on which structural features are essential for binding. As shown in Figure 3-10 A and B, there are two types of mammalian GalCer, type I, with a 2-hydroxy fatty acid, and type II, which has a non-hydroxylated fatty acid. The importance of the hexose moiety in the reactivity of MsDef1 with GSLs was clearly confirmed from this experiment. A mixture of mammalian GalCer type I and II was used in this experiment, and no reactivity was observed at any concentrations. The main difference between plant GlcCer and mammalian GalCer-I is the hexose moiety (Figure 3-9 C and 3-10 A). Both of these GSLs have a saturated 2-hydroxy fatty acid. The fact that plant GlcCer

61

shows reactivity and mammalian GalCer-I do not suggests that presence of glucose in the GSL structure is the important feature determining the binding specificity. The possibility of a 2-hydroxy group on the fatty acid alone being the structural determinant in MsDef1 recognition is discarded by this result, since mammalian GalCer-I presents a 2-hydroxy fatty acid but did not show any binding.

Among the various fungal GlcCer employed in the study, GlcCer from *F.graminearum, A.fumigatus, and N.crassa* express ceramides with Δ^3 unsaturated fatty acids, while *A. bisporus* has a saturated fatty acyl component (Figure 3-9 A and B). Since all fungal GlcCer showed reactivity towards MsDef1 without any significant differences, it appears that the fatty acyl-Δ^3-unsaturation of ceramide does not have any influence on determining the binding specificity. Plant GlcCer express ceramide with a saturated 2-hydroxy fatty acid component, which is the same as the ceramide in *A.bisporus*. The main structural difference observed between plant and fungal GlcCer is the 9-methyl substituent on the sphingoid chain of fungal ceramides, which plants lack (Figure 3-9 B and C). Both plant and fungal GlcCer spare Δ^8 –unsaturation of the sphingoid. In the ELISA assay, both plant and fungal GlcCer showed binding to MsDef1. This observation suggests that the 9-methyl substituent on the sphingoid chain of ceramide is also not likely to be an important structural feature governing the binding.

Mammalian GlcCer shows a number of structural differences from plant and fungal GlcCer such as lack of fatty acyl Δ^3-unsaturation, 9-methyl substitution

62

on the sphingoid, Δ^8-unsaturation of the sphingoid, and 2-hydroxyl substitution on fatty acid. In the ELISA assay, MsDef1 reacted effectively with plant GlcCer, which has a saturated hydroxylated fatty acyl component, but did not react with mammalian GlcCer, which present a saturated non-hydroxylated fatty acid (Figure 3-9 C and D). Since the fatty acyl Δ^3-unsaturation and sphingoid 9-methyl branch already appear to be non-required features, this result suggests that the 2-hydroxy group of the fatty acid is an important feature governing the MsDef1 binding to GlcCer. However, another structural difference between mammalian and other GlcCer is the Δ^8-unsaturation of the sphingoid, which is present in both plants and fungi. From the available results, it is not clear whether this Δ^8-unsaturation is involved in the recognition of GlcCer by Msdef1, but we speculate that since this structural feature is far away from the main binding epitope it may not have any influence in the interaction between MsDef1 and GlcCer. Consistent with this, the 9-methyl substitution on the sphingoid chain, which is also far away from the epitope, is not relevant for the binding to occur. Structural features such as 9-methyl substitution and Δ^8-unsaturation of the sphingosine are likely to be embedded in the cell membrane, and presumably do not have significant effects on binding specificity. From these results it was concluded that the minimum epitope required for optimum binding of MsDef1 with GlcCer would comprise the presence of a β-D-glucose residue and the 2-hydroxy group of the fatty acid. Other structural variations observed do not appear to have any relevance governing binding specificity of MsDef1 with GlcCer.
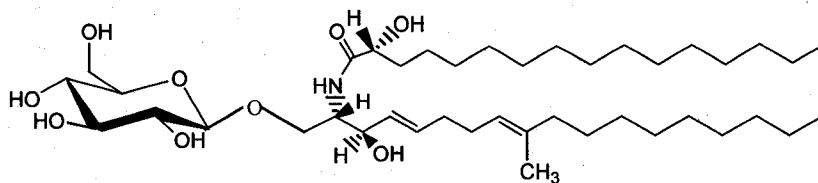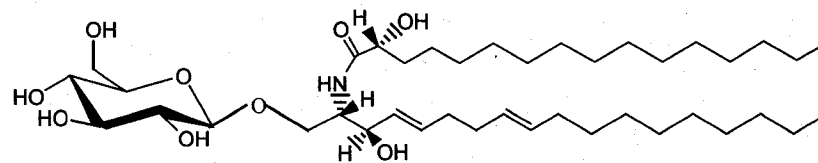
63

A
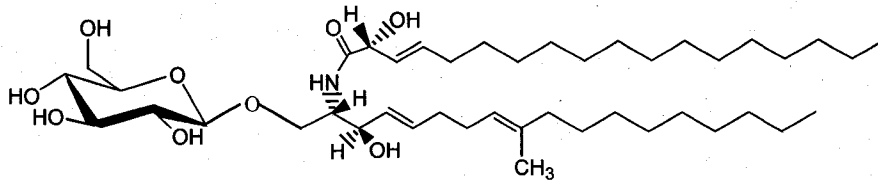
h18:1
d18:2

F.gram./A.fmgs./N.cras - GlcCer

B

h16:0
d18:2

A.bisporus - GlcCer

C
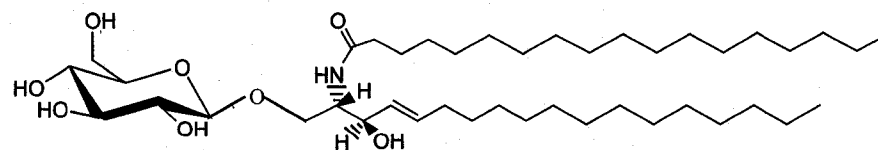
h16:0
d18:2

Plant GlcCer

D

h18:0
d18:1

Mammalian GlcCer

Figure 3-9: Various GlcCer showing structural variations in the ceramide moiety.

64

A

Mammalian GalCer-I

h18:0
d18:1

B

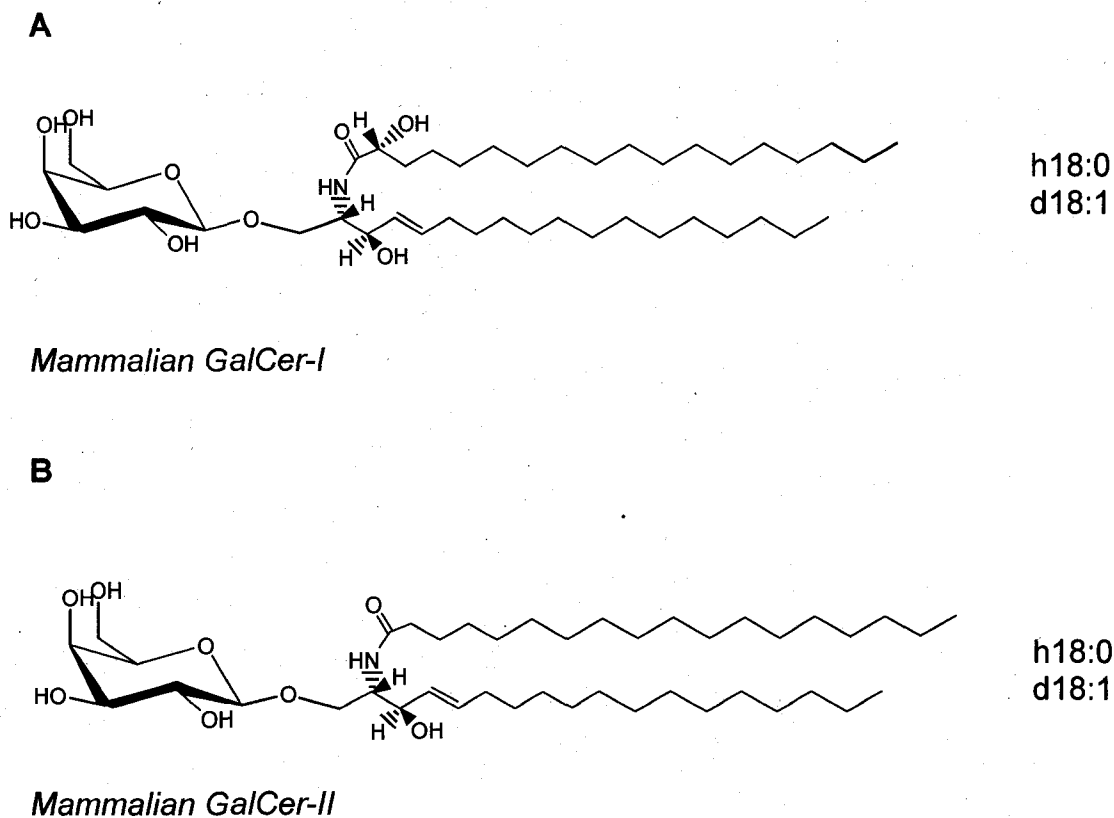

Mammalian GalCer-II

h18:0
d18:1

Figure 3-10: Mammalian GalCer types I and II showing structural variations in the ceramide moiety. Type I has 2-hydroxy fatty acid.

Another ELISA experiment was conducted employing another defensin named MtDef4, which is also from *Medicago* spp. and has shown strong antifungal activity. MtDef4 shares 41% identity in amino acid sequences with MsDef1 [38, 39]. Even though defensins vary greatly in their amino acid composition, they all have a compact shape that is stabilized by either four or five intramolecular disulfide bonds. In this experiment the binding specificity of MtDef4 with GlcCer from *N.crassa* and plant origin, along with mammalian GlcCer and GalCer, were compared. As a positive control, MsDef1 was also

65

used with the same set of GSLs. Resulting binding curves are shown in Figure 3-11.

ELISA - II - MsDef1 & MtDef4

Legend:
- N.cras + MsDef1
- plant GlcCer +MsDef1
- mam.GlcCer + MsDef1
- mam.GalCer + MsDef1
- N.cras +MtDef4
- plant GlcCer + MtDef4
- mam.GlcCer + MtDef4
- mam.GalCer +MtDef4
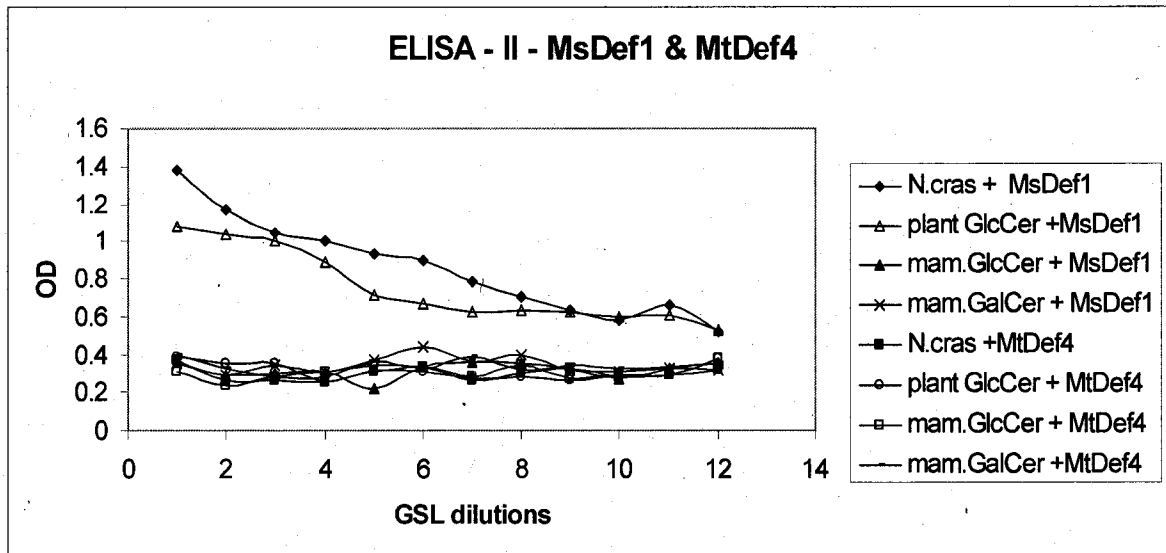
Axes: OD (y-axis), GSL dilutions (x-axis)

Figure 3-11: Binding curves showing reactivity of MsDef1 and MtDef4 with varying concentrations of GSLs

As expected, MsDef1 showed specific binding to *N.crassa* and plant GlcCer in a concentration dependent manner, and did not react with mammalian GlcCer and GalCer. However, MtDef4 did not react with any of the GSLs at any concentration. From this observation we can suggest that the antifungal activity of MtDef4 is probably not be based on interaction with GlcCer or GalCer. At this point we do not have any information on whether any components of the cell membrane have a role in MtDef4 recognition. The mode of antifungal action of MtDef4 will need to be established by further research.

66

MALDI-TOF MS Analysis

The molecular mass and expected disulfide bridging of the defensin (MsDef1) preparation we are using was confirmed by MALDI-MS analysis. The monoisotopic singly charged parent ion mass of MsDef1, calculated from the complete amino acid sequence, is 5192.2469 Da. The calculated average molecular mass for MsDef1 is 5195.8815 Da. In the theoretical isotope distribution, the *m/z* of the tallest peak is also predicted to be at *m/z* 5195. However, MsDef1 has eight cysteine residues and forms four disulfide bridges in its native folded state. Therefore, in the folded state, the monoisotopic mass of MsDef1 is predicted to be 5184.1845 Da, and the average molar mass is predicted to be 5187.8175 Da (with the loss of eight hydrogens while forming four disulfide bridges). Figure 3-12 shows the MALDI-MS profile obtained for MsDef1; an isotope cluster with the tallest peak was observed at *m/z* 5187. This is consistent with the average molecular mass of MsDef1 with all four disulfide bonds intact.
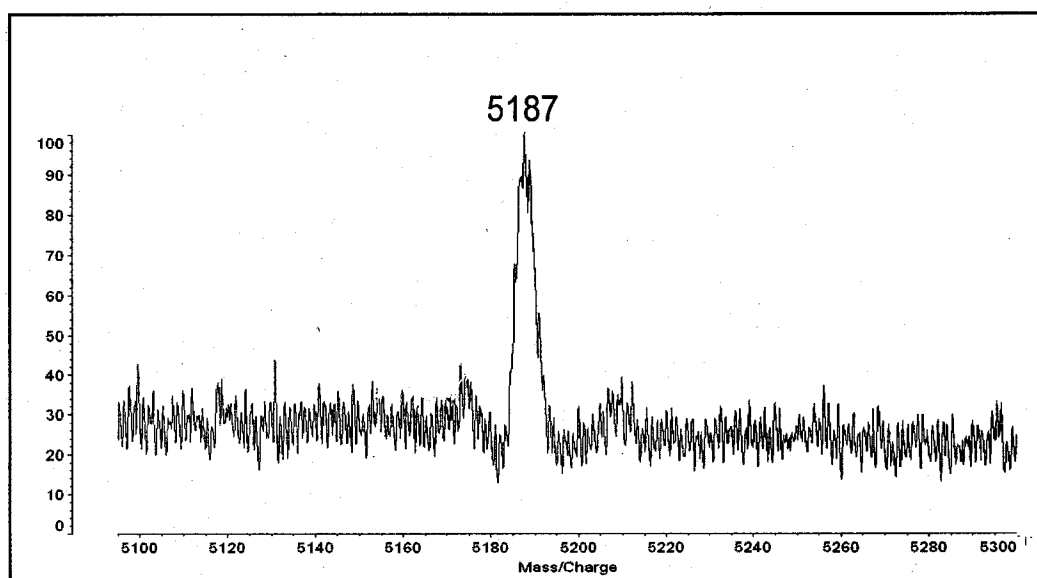
Figure 3-12: MALDI -MS of MsDef1 showing the singly charged molecular ion of average mass 5187 Da.

When a mixture of MsDef1 and GlcCer from *N. crassa* was subjected to MALDI - MS analysis no significant peaks were detected in the anticipated region of the mass spectrum. Mixtures of MsDef1 and GlcCer in varying concentrations were analyzed with two different matrices (α-cyano-4-hydroxy cinnamic acid and dihydroxybenzoic acid). We speculate that the complex molecules could not be preserved and detected due to the energy impact during the ionization process with the matrices and experimental conditions employed. Excess salt on the target surface, resulting from the dried buffer, could also interfere with detection. These experimental conditions could perhaps be optimized to enable the detection of the MsDef1- GlcCer complex.

It is worth noting that MALDI has been much less frequently applied to study non-covalent complexes. The sample preparation process for MALDI, that

68

is, crystallizing the analyte with a large molar excess of organic chromophore, could to be denaturing for many proteins, so that only the most stable non-covalent complexes could be preserved and ultimately detected. The co-crystallization step includes complex physical and chemical processes involving interactions of the analyte with matrix molecules in solution and after crystallization. Many attempts have been made to detect intact complexes using MALDI; however, no significant trends can be drawn for a general protocol on the target preparation process [44, 45, 46]. Thus the failure to detect a non-covalent complex ion in a MALDI spectrum does not necessarily allow conclusions to be drawn regarding hypothesized interactions.

ESI - MS Analysis

Electrospray ionization has long been recognized as the method of choice for studying non-covalent antibody-peptide complexes [47]. ESI experiments can be carried out using aqueous solutions containing volatile buffers to maintain physiological pH, ionic strength, or other conditions that preserve the integrity of the complex in solution. Ion generation from a solution is quite natural for protein complexes, and particular conditions have been found to preserve the weak protein associations. In addition, electrostatic and dipolar interactions are strengthened in the absence of solvent, allowing the generation and detection of very large intact complex ions [48, 50]. Noncovalent complexes between proteins and lipids have also been studied successfully. The advantages of ESI-MS also include high selectivity and sensitivity along with speed of analysis. A variety of protocols has been devised to validate specificity of interactions [47].

69

Figure 3-13 shows ESI-MS spectra of MsDef1 and GlcCer from *N.crassa* (Panels A and B, respectively). Triply and quadruply charged ions, ([M+3H]$^{3+}$ and [M+4H]$^{4+}$), for MsDef1 were observed at *m/z* 1729 and 1297 respectively (Figure 3-13 A); doubly charged ion (predicted at *m/z* 2593) is beyond the *m/z* range of the instrument. As expected the GlcCer fraction from *N. crassa* showed a sodiated molecular ion profile with the most abundant peak at *m/z* 776 and a much less abundant peak at *m/z* 778 (overlapped with M+2 isotope peak for *m/z* 776) [30, 34]. These are consistent with [M + Na]$^{+}$ adducts of GlcCer containing two ceramide types, each having a d18:2 sphingoid chain, with h18:1 and h18:0 fatty acid respectively (Figure 3-13 B). It appears from this spectrum that the Δ^3-unsaturated fatty acid form is greatly predominant in this GlcCer fraction.
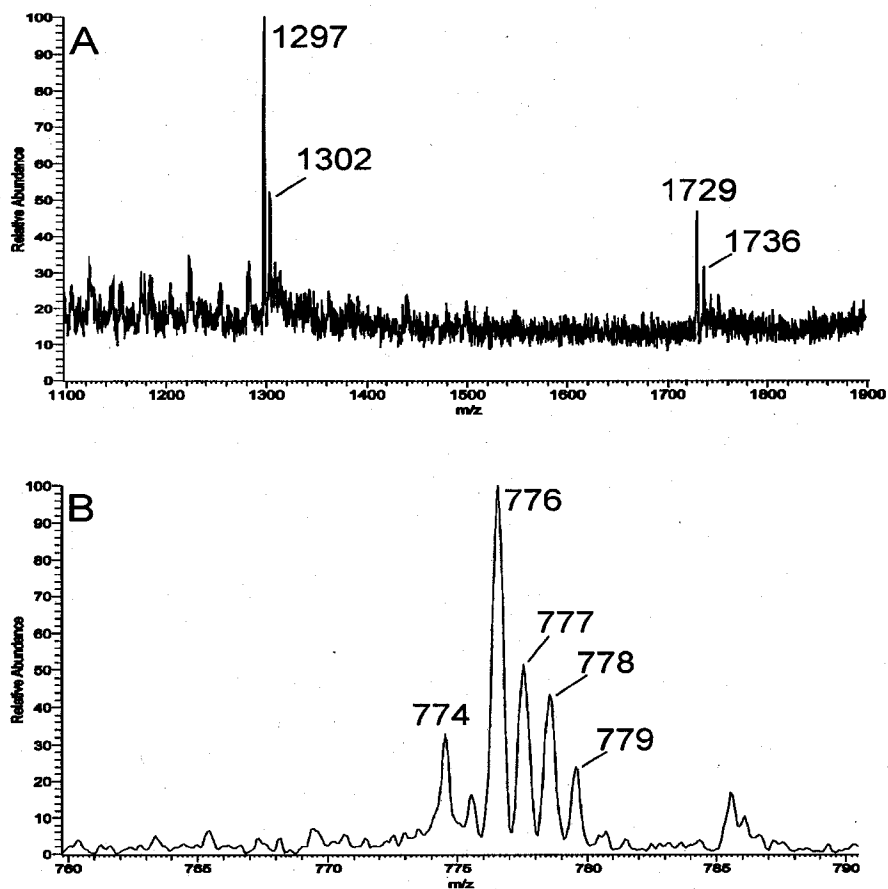
70

Figure 3-13: ESI-MS of MsDef1 in buffer (A) showing the [M+3H]$^{3+}$ and [M+4H]$^{4+}$ molecular ions at *m/z* 1729 and 1297 respectively (A) and the [M + Na]$^{+}$ adduct of GlcCer from *N.crassa* (B)

Analysis of a solution containing a 1:1 mixture of MsDef1 and GlcCer showed an isotopic cluster with the tallest peak at *m/z* 1485, as shown in Figure 3-14. A quadruply charged MsDef1-GlcCer complex ion, [M+4H]$^{4+}$, is predicted to be at *m/z* 1486, which is consistent with the observed peak. If the complex were detected as a fully sodiated adduct, the [M+4Na]$^{4+}$, it is predicted to appear

71

at *m/z* 1508. However, it is an unlikely form for what is mainly protein. Further experiments will need to be carried out to characterize the MsDef1-GlcCer complex observed at *m/z* 1486. A low energy CID- MS^2 analysis could possibly reveal whether the species observed at *m/z* 1486 includes a bound GlcCer. Less abundant peaks of non-bound MsDef1 at *m/z* 1297 ([M+4H]$^{4+}$) and GlcCer at *m/z* 776 were also detected from the mixture.
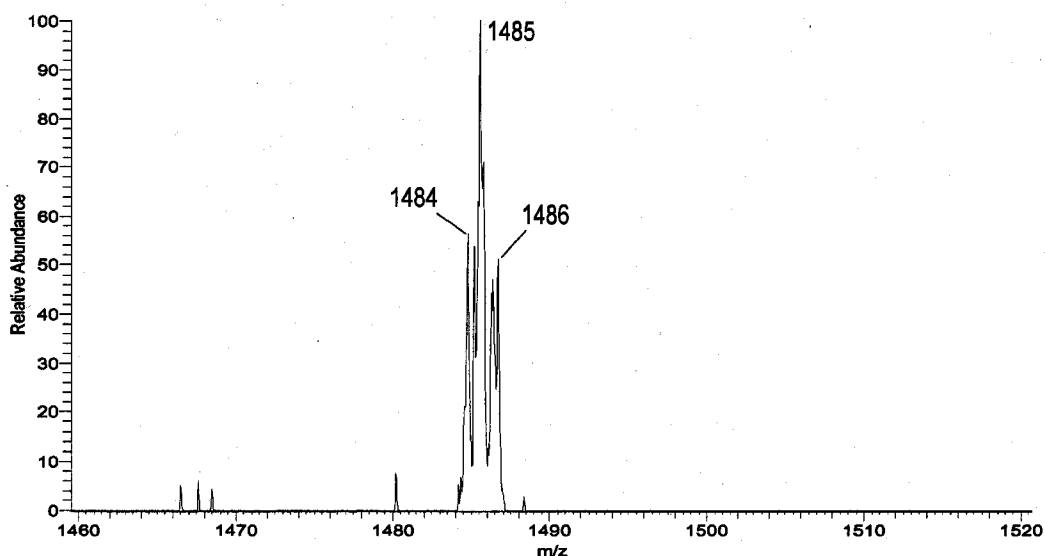

Figure 3-14: ESI-MS of MsDef1 – GlcCer mixture showing the abundant ion at *m/z* 1486.

Some analytes tend to form non-covalent gas phase assemblies, despite the nonexistence of the corresponding complexes in solution. The role MS plays in characterizing noncovalent complexes is entirely complimentary to other techniques, but can still be useful [47]. The fact that different types of

72

intermolecular forces appear to be of different relative importance in maintaining complexes in the gas and solution phases suggest that their comparison can provide important insights into the nature of the interaction between a protein and its ligands.

Conclusion and Future work

It should be noted that in this project only preliminary experiments were conducted to detect a bimolecular complex by mass spectrometry. At this point, it appears that we have been successful, but many additional experiments could be performed to reach the initial goal of characterizing the complex. Once detected, considerable work remains to verify that it is specific and meaningful. A low energy CID- MS^2 analysis of the complex should reveal whether the species observed includes a bound GlcCer. It would also be of considerable interest to see if the pattern of recognition of GSL structural variations by MsDef1, as observed in the ELISA experiments, could be recapitulated by differential detection of complexes in ESI-MS. For example, would the observation that MsDef1 recognized fungal and plant GlcCer, but did not bind to mammalian GlcCer and GalCer, be repeatable using MS methods. Other more established techniques, such as crystallography and NMR, could also be tried to provide more details into the possible structure of a bimolecular MsDef1-GlcCer complex.

73

LIST OF REFERENCES

1. Kolter, T.; Sandhoff, K. *Angew. Chem. Int. Ed .Engl.* **1999**, *38*, 1532-1568.

2. Dickson, R. C. *Annu. Rev. Biochem.* **1998**, *67, 27-48.*

3. Dickson, R. C.; Lester, R. L. *Biochim. Biophys. Acta* **1999**, *1438*, 305-321.

4. Dickson, R.C.; Lester, R. L. *Biochim. Biophys. Acta* **2002**, *1583*, 13-25.

5. Thevissen, K.; Francois, E. J. A.; Takemoto,Y. J.; Ferket, K. A.; Meert, E. K.; Cammue, B. P. A. *J.Biol.Chem.***1996**, *271*, 15018-15025.

6. Thevissen, K.; Francois, E. J. A.; Takemoto,Y. J.; Ferket, K. A.; Meert, E. K.; Cammue, B. P. A.*FEMS Microbiology Letters* **2003**, *226*, 169-173.

7. Thevissen, K.; Baldys, J. I.; Yang, J. I.; Takemoto,Y. J.; Francois, E. J. A.; Aerts, A. M.; Ferket, K. A.; Meert, E. K.; Winderickx, J.; Roosen, J.; Cammue, B. P. A. *FEBS Letters* **2005**, *579*, 1973-1977.

8. Aerts, A. M.; Francois, E. J. A.; Bammens, L.; Cammue, B. P. A.; Smets, B.; Winderickx, J.; Accardo, S.; DeVos, E. D.; Thevissen, K. *FEBS Letters* **2006**, *580*, 1903-1907.

9. Thevissen, K.; Cammue, B. P. A.; Lemaire, K.; Winderickx, J.; Dickson, R. C.; Lester, R. L.; Ferket, K. A.; Even, V. F.; Parret, H. A.; Broekaert, F. W. *Proc. Natl. Acad. Sci.* **2000**, *97*, 9531-9536.

10. Watanabe, R.; Funato, K.; Venkataraman, K.; Futerman, H. A.; Riezman, H. *J. Biol. Chem.* **2002**, *277*, 49538-49544.

11. Meier, D. K.; Deloche, O.; Kentaro, K.; Funato, K.; Riezman, H. *Molecular Biology of the Cell* **2006**, *17*, 1164 -1175.

12. Liu, K.; Zhang, X.; Lester, R. L.; Dickson, R. C. *Biochem. Soc.Transactions* **2005**, *33*, 1170-1173.

13. Toledo, M. S.; Levery, S. B.; Straus, A. H.; Takahashi, H. T. *FEBS Letters* **2001**, *493*, 50-56.

14. Levery, S. B.; Momany, M.; Lindsey, R.; Toledo, M. S.; Shayaman, J. A.; Fuller, M.; Brooks, K.; Doong, R. L.; Straus, A. H.; Takahashi, H. T.; *FEBS Letters* **2002**, *525*, 59-64.

15. Toledo, M. S.; Levery, S. B.; Glushka, J.; Straus, A. H.; Takahashi, H. T. *Biochem. Biophys. Res. Commun.* **2001**, *280*, 19-24.

16. Levery, S. B.; Toledo, M. S.; Straus, A. H.; Takahashi, H. T. *J. Biochemistry* **1998**, *37*, 8764-8775.

17. Toledo, M. S.; Levery, S. B.; Bennion, B.; Guimaraes, L. L.; Castle, S. A.; Lindsey, R.; Momany, M.; Park, C.; Straus, A. H.; Takahashi, H. T. *J. Lipid Research* **2007**, *48*, 1-23.

18. Levery, S. B.; Toledo, M. S.; Doong, R. L.; Straus, A. H.; Takahashi, H. T. *Rapid Commun. in Mass Spectrom.* **2000**, *14*, 551-563.

19. Levery, S. B.; Toledo, M. S.; Straus, A. H.; Takahashi, H. T. *Rapid Commun. in Mass Spectrom.* **2001**, *15*, 2240-2258.

20. Hsu, F. F.; John, T. *J. Am. Soc. Mass Spectrometry* **2001**, *12*, 61-79.

21. Riezman, H. *Biochemical Society* **2006**, 367-369.

22. Thomma, P. H. J.; Cammue, B. P. A.; Thevissen, K. *Planta* **2002**, *216,193*-202.

23. Brade, L.; Vielhaber, G.; Heinz, E.; Brade, H. *Glycobiology* **2000**, *10*, 629-636.

24. Thevissen, K.; Ferket, K. A.; Francois, E. J. A.; Cammue, B. P. A. *Peptides* **2003**, *24*, 1705-1712.

25. Thevissen, K.; Warnecke, C. D.; Francois, E. J. A.; Leipelt, M.; Heinz, E.; Ott, C.; Zahringer, U.; Thomma, P. H. J.; Ferket, K. A.; Cammue, B. P. A.; *J. Biol. Chem.* **2004**, *279*, 3900-3905.

26. Spelbrink, G. R.; Dilmac, N.; Allen, A.; Smith, T. J.; Shah, M.D. *Plant Physiology,* **2004**, *135*, 2055-2067.

27. Thevissen, K.; Terras, F. G.; Broekaert, W. F. *Applied and Environmental Microbiology* **1999,** *65*, 5451-5458.

28. Thevissen, K.; Ghazi, A.; Samblanx, G. W.; Brownlee, C.; Osborn, R. W.; Broekaert, W. F. *J. Biol. Chem.* **1996**, *271*, 15018-15025.

29. Ferket, K. A.; Levery, S. B.; Park, C.; Cammue, B. P. A.; Thevissen, K. *Fungal Genetics and Biology* **2003**, *40,176*-185.

75

30. Park, C.; Bennion, B.; Francois, E. J. A.; Ferket, K. A.; Cammue, B. P. A.; Thevissen, K.; Levery, S. B. *J. Lipid Research*, **2005**, *46*,759-768.

31. Stine, R.; Pishko, V.M.; *Anal. Chem.* **2005**, *77*, 2882-2888.

32. Bennion, B.; Park, C. Fuller, M.; Lindsey, R.; Momany, M.; Jennemann, R.; Levery, S. B. *J. Lipid Research* **2003**, *44*, 2073-2088.

33. Toledo, M.S.; Suzuki, E.; Levery, S. B.; Straus, A.H.; Takahashi, H.T. *Glycobilogy* **2001**, *11*, 105-112.

34. Toledo, M. S.; Levery, S. B.; Straus, A. H.; Suzuki, E.; Momany, M.; Glushka, J.; Moulton, J.; Takahashi, H. T. *J. BioChemistry.* **1999**, *38*, 7294-7306.

35. Barreto-Bergter, E.; Rodriguez, M. L.; Pinto, R. M. *An. Acad. Bras. Cien.* **2004**, *76*, 67-84.

36. Val, F.; Andrivon, D.; Desender, S. *Cellular Microbiology*, **2007**, *9*, 21-30.

37. Robatzek, Silke.; *Cellular Microbiology* **2007**, *9*, 1-8.

38. Ramamoorthy, V.; Cahoon, E. B.; Jia, L.; Thokala, M.; Minto, R. E.; Shah, M. D. *Mol. Microbiol.* **2007**, *66*, 771-786.

39. Ramamoorthy, V.; Zhao, X.; Snyder, A. K.; Jinrong, X.; Shah, M. D. *Cellular Microbiology* **2007**, *9*, 1491-1506.

40. Robinson, C. V.; Chung, E. W.; Kragelund, B. B.; Knudsen, J.; Aplin, R. T.; Poulsen, F. M.; Dobson, C. M. *J. Am. Chem. Soc.* **1996**, *118*, 8646-8653.

41. Robinson, C. V.; Benesch, J. L. P. *Current Opinion in Structural Biology* **2006**, *16*, 245-251.

42. Zhang, S.; Colleen, K. V. P.; Wilson, D. B. *Anal. Chem.* **2003**, *75*, 3010-3018.

43. Clark, S. M.; Konermann, L. *Anal. Chem.* **2004**, *76*, 1257-1263.

44. Bolbach, Gerard. *Current Pharm. Design* **2005**, *11*, 25-35-2557.

45. Downard, K. M.; Kiselar, J. G.; *J. Am. Soc. Mass Spectrom.* **2000**, *11*, 746-750.

46. Downard, K. M.; Kiselar, J. G.; *Anal. Chem.* **1999**, *71*, 1792-1801.

47. Loo, J. A.; *Mass Spectrom. Rev.***1997**, *16*, 1-23.

48. Robinson, C.V.; Leopold, L. I.; Malo, J.; Hatters, D. M.; Howlett, G. J. *Biophysical Journal* **2003**, *85*, 3802-3812.

49. Schlosser, G. *Rapid Commun. in Mass Spectrom.* **2003**, *17*, 2741-2747.

50. Heck, A. J.; Pinske, W. M. *J. Am. Soc. Mass Spectrom* **2004**, *15,* 1392-1399.

51. Wells, G. B.; Lester, R. L. *J. Biol. Chem.* **1983**, *258*, 10200-10203.

52. Smith, W. S.; Lester, R. L. *J. Biol. Chem.* **1974**, *249,* 3395-3405.

53. Lester, R. L.; Dickson, R. C. *Advances in Lipid Research*, **1993**, *26,* 253-274.

APPENDICES

DOWNFIELD SECTIONS OF ^{1}H – ^{13}C gHSQC NMR SPECTRA OF MIPC AND M(IP)$_2$C

^{1}H – ^{13}C gHSQC - MIPC
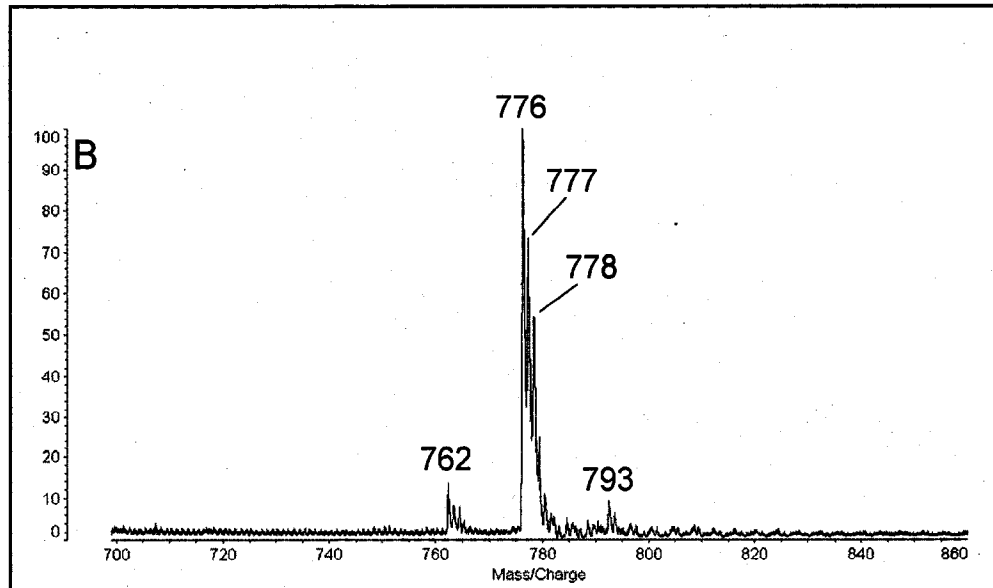

79
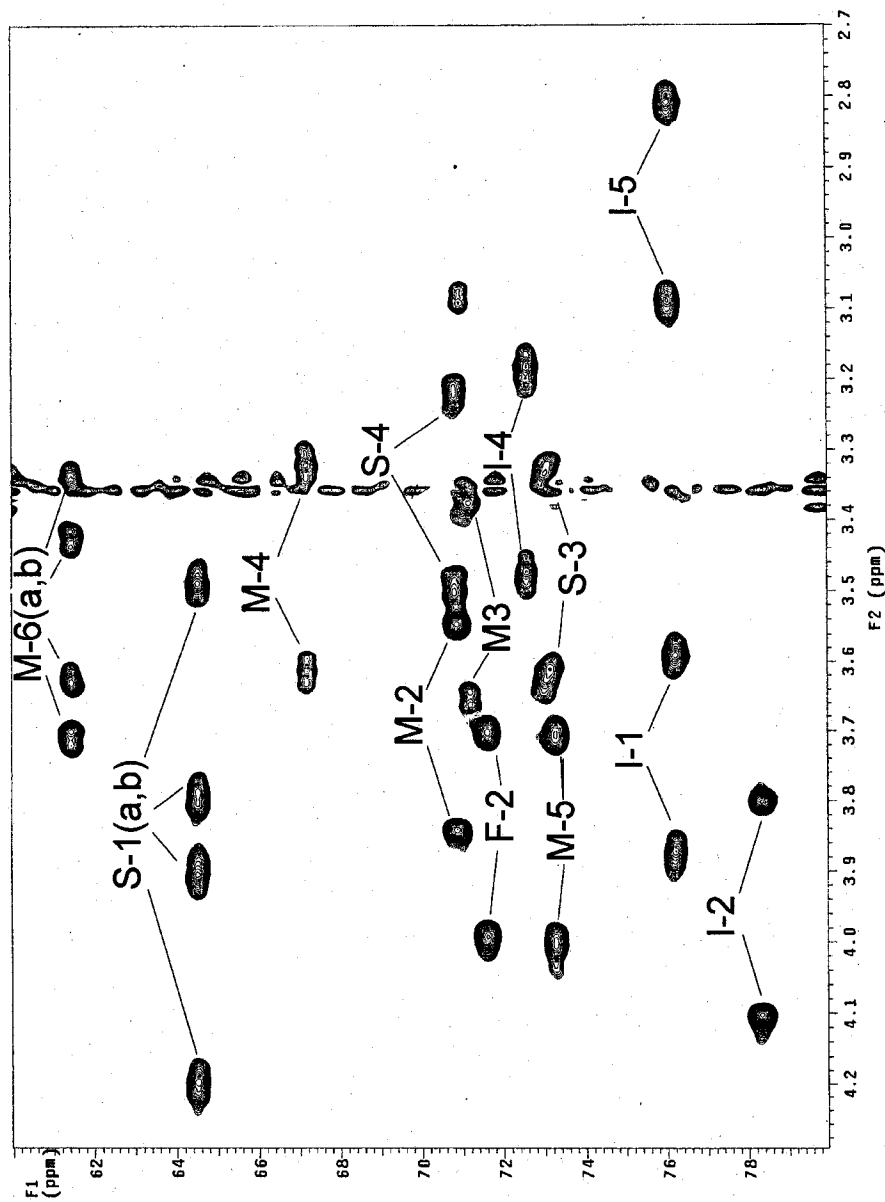
^{1}H – ^{13}C gHSQC – M(IP)$_2$C
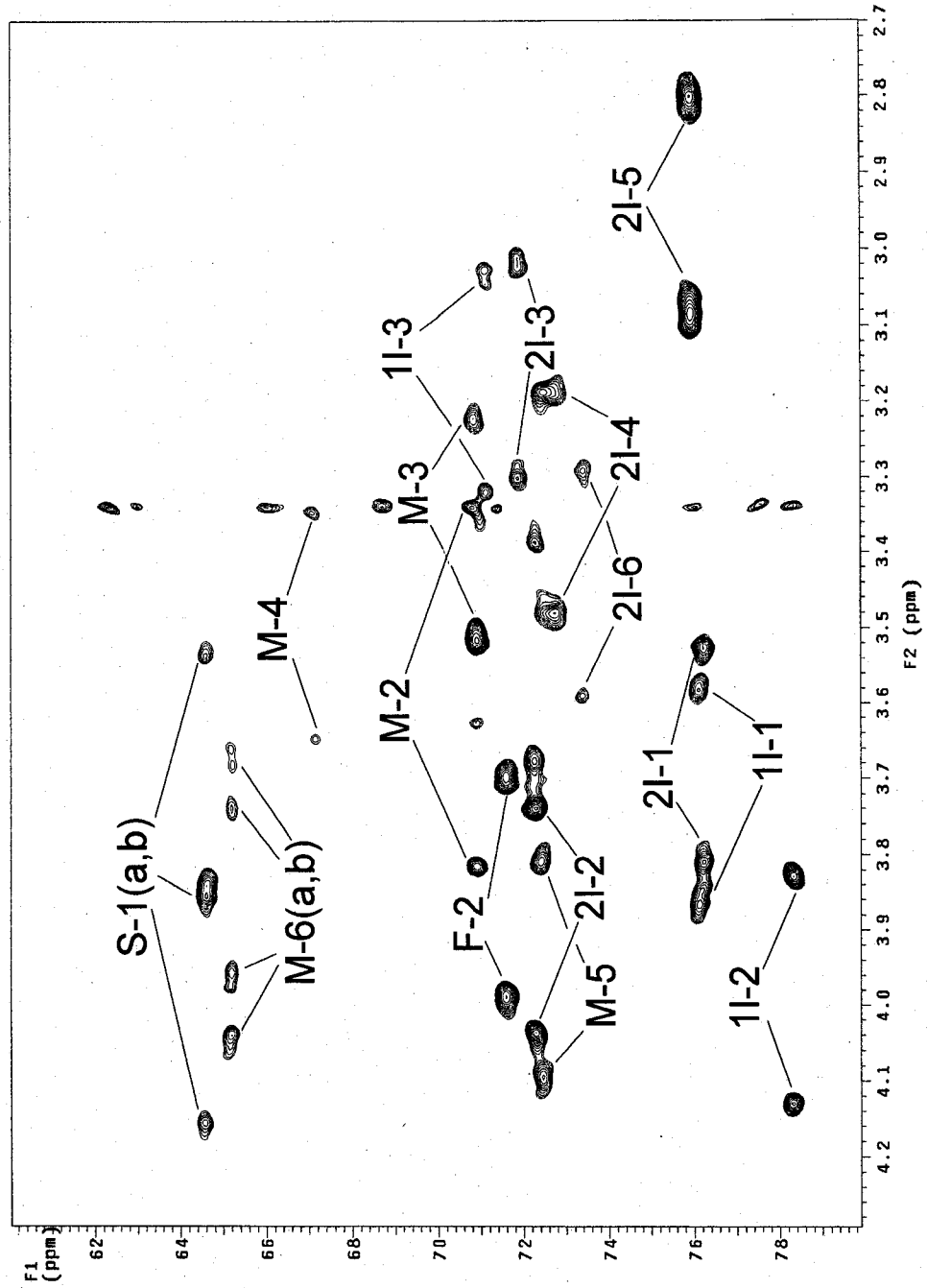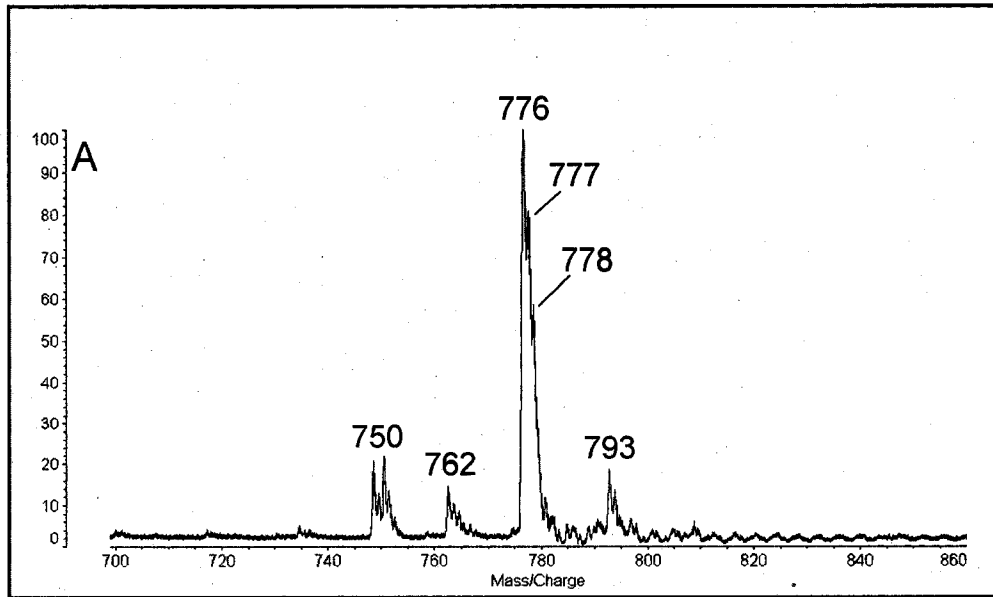
MALDI – MS SPECTRA OF GSLs USED IN ELISA Experiments

GlcCer from _F.graminearum_ (A) and _A.bisporus_ (B)

81
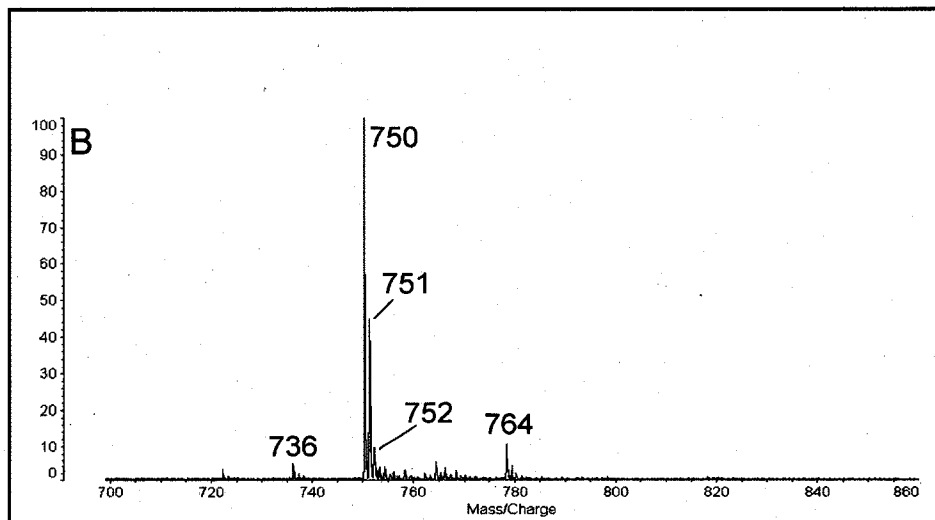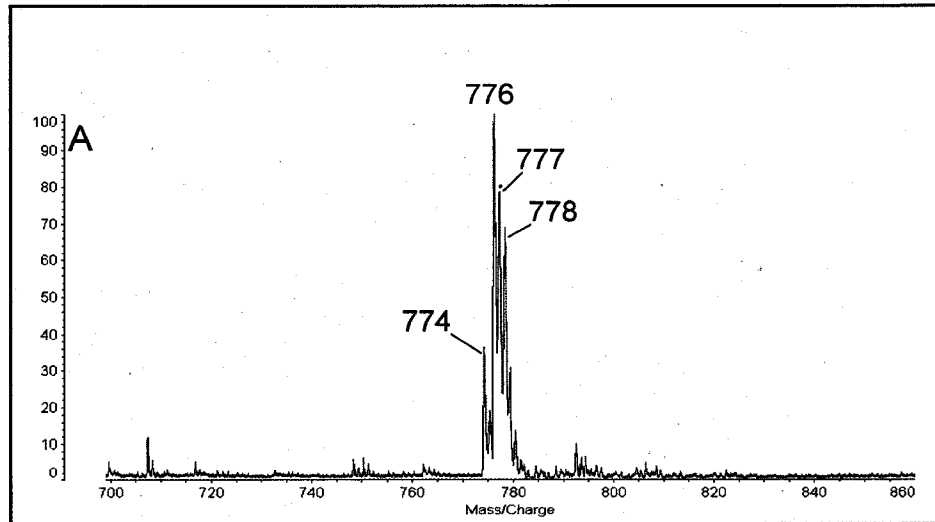
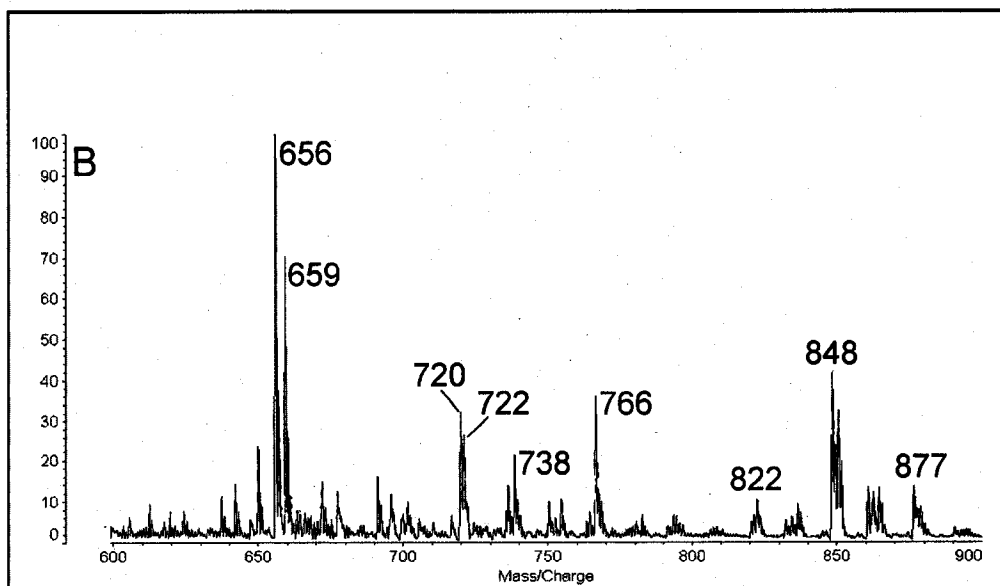GlcCer from *N. crassa* (A) and *A. fumigatus* (B)

Mammalian GlcCer (A) and mammalian GalCer (B)
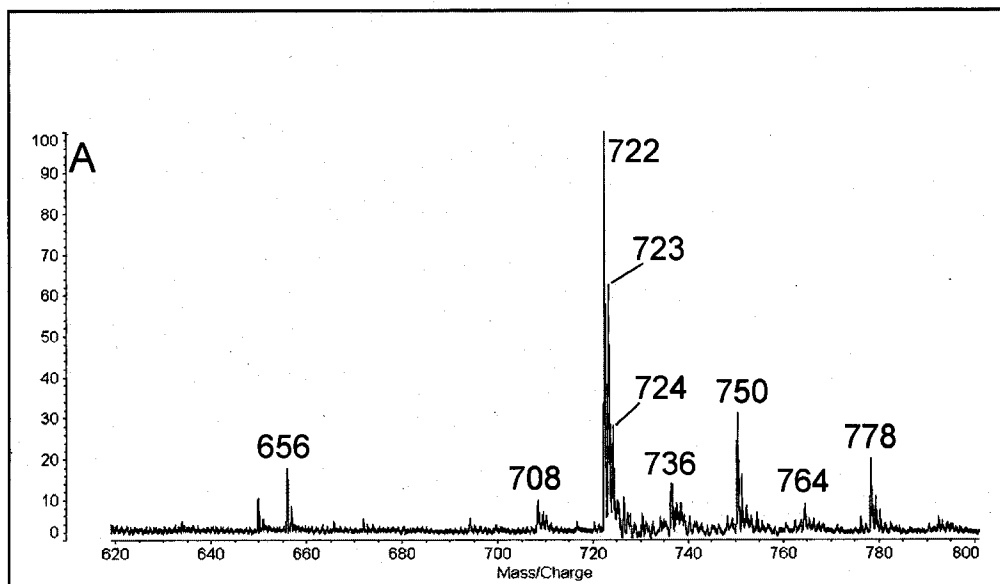
GlcCer from plant origin (soybean)